Neuron

Article

Gut-brain cholinergic signaling mediates the antiseizure effects of *Bacteroides fragilis*

Graphical abstract

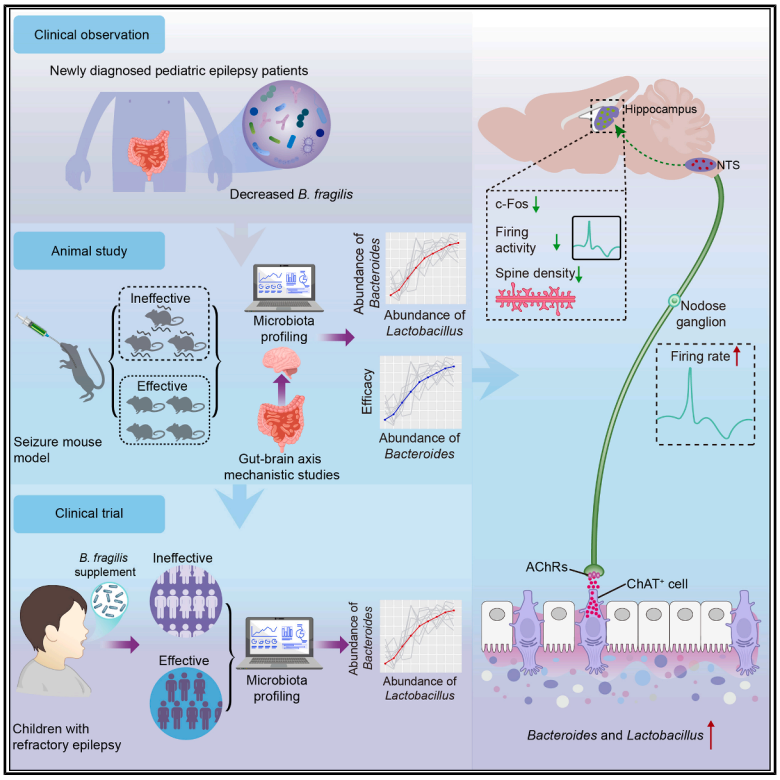

Highlights

- *Bacteroides fragilis* suppresses seizures via vagal gut-brain cholinergic signaling
- It activates colonic ChAT$^+$ cells to enhance acetylcholine-mediated vagal transmission
- Antiseizure effects associate with enriched intestinal *Lactobacillus* colonization
- A clinical trial confirms antiseizure efficacy in pediatric refractory epilepsy

Authors

Yicong Jia, Hong Chen, Qianhui Zou, ..., Zuxin Chen, Dezhi Cao, Xin-an Liu

Correspondence

zx.chen3@siat.ac.cn (Z.C.), caodezhi888@aliyun.com (D.C.), xa.liu@siat.ac.cn (X..-a.L.)

In brief

Jia et al. show that the antiseizure effects of *Bacteroides fragilis* are mediated by enhanced cholinergic signaling along the gut-vagus-brain axis and reinforced by the gut colonization of *Lactobacillus*. These findings reveal a microbiota-neural circuit interaction with translational implications for pediatric refractory epilepsy.

Jia et al., 2026, Neuron *114*, 1–24
March 18, 2026
https://doi.org/10.1016/j.neuron.2025.11.029

CellPress

Please cite this article in press as: Jia et al., Gut-brain cholinergic signaling mediates the antiseizure effects of *Bacteroides fragilis*, Neuron (2025), https://doi.org/10.1016/j.neuron.2025.11.029

Neuron

CellPress

Article

Gut-brain cholinergic signaling mediates the antiseizure effects of *Bacteroides fragilis*

Yicong Jia,[1,5,9] Hong Chen,[2,9] Qianhui Zou,[1,6] Sijing Chen,[5] Jiahao Li,[1] Yiming Chen,[8] Liming Lu,[8] Feng Hong,[1] Shuhui Jia,[1,3] Xiaoyuan Jing,[1,3] Jiayan Ren,[3,4] Fahim Muhammad,[3,4] JiaYu Mi,[2] Jing Duan,[2] Jianxiang Liao,[2] Qing Liu,[1,3,6] Fuqiang Xu,[1,3,6] Paul J. Kenny,[7] Ming-Hu Han,[1,3] Liping Wang,[1,3,6] Zuxin Chen,[1,3,4,6,*] Dezhi Cao,[2,*] and Xin-an Liu[1,3,6,10,*]

[1]Guangdong Provincial Key Laboratory of Brain Connectome and Behavior, the Brain Cognition and Brain Disease Institute, Shenzhen Institutes of Advanced Technology, Chinese Academy of Sciences, Shenzhen 518055, China

[2]Neurology Department, Shenzhen Children's Hospital, Shenzhen 518055, China

[3]Shenzhen-Hong Kong Institute of Brain Science, Shenzhen Institutes of Advanced Technology, Chinese Academy of Sciences, Shenzhen 518055, China

[4]Shenzhen Key Laboratory of Drug Addiction, Shenzhen Neher Neural Plasticity Laboratory, the Brain Cognition and Brain Disease Institute, Shenzhen Institutes of Advanced Technology, Chinese Academy of Sciences, Shenzhen 518055, China

[5]State Key Laboratory of Biocatalysis and Enzyme Engineering, School of Life Sciences, Hubei University, Wuhan, China

[6]University of Chinese Academy of Sciences, Beijing 100049, China

[7]Nash Family Department of Neuroscience, Icahn School of Medicine at Mount Sinai, New York, NY 10029, USA

[8]South China Research Center for Acupuncture and Moxibustion, Guangzhou University of Chinese Medicine, Guangzhou, China

[9]These authors contributed equally

[10]Lead contact

*Correspondence: zx.chen3@siat.ac.cn (Z.C.), caodezhi888@aliyun.com (D.C.), xa.liu@siat.ac.cn (X.-a.L.)

https://doi.org/10.1016/j.neuron.2025.11.029

SUMMARY

Gut dysbiosis has been implicated in epilepsy, yet probiotic efficacy and mechanisms remain unclear. Here, we identify that *Bacteroides fragilis* (*B. fragilis*) is markedly reduced in children with epilepsy and show that oral *B. fragilis* administration suppresses seizures in both pentylenetetrazole- and kainic-acid-induced mouse models. Mechanistically, *B. fragilis* activates colonic choline acetyltransferase-positive ($ChAT^+$) cells and enhances gut-vagus-brain cholinergic signaling, as demonstrated by vagal recordings, pharmacological blockade, and chemogenetic manipulation, identifying a colonic $ChAT^+$-nodose ganglion circuit mediating seizure suppression. Its antiseizure effects associate with enriched intestinal *Lactobacillus* colonization. A randomized clinical trial (CHiCTR2100042203) further confirms the therapeutic efficacy of *B. fragilis* in pediatric refractory epilepsy. These findings define a gut-brain cholinergic pathway through which *B. fragilis* exerts antiseizure effects and establish a mechanistic basis for microbiota-targeted therapies in epilepsy.

INTRODUCTION

Pediatric epilepsy is among the most prevalent neurological disorders in children, often disrupting development and characterized by recurrent seizures. Approximately 10%–30% of patients develop refractory epilepsy, underscoring the urgent need for effective and safe therapeutic interventions.[1–5]

The gut microbiota critically modulates host physiology and behavior across the lifespan.[6–9] Increasing evidence links microbial dysbiosis to neurodevelopmental disorders, including autism spectrum disorder and pediatric epilepsy.[10–12] Emerging research from both animal models and clinical cases points to a potential link between gut dysbiosis and specific forms of epilepsy.[11,13,14] Non-pharmacological interventions such as the ketogenic diet (KD) have shown efficacy in managing refractory epilepsy in children.[14] Although studies on microbiota-based therapies—such as fecal microbiota transplantation, KD, and probiotics—remain limited, they offer promise, especially when conventional treatments are ineffective or cause adverse effects.[13–15] Their efficacy, however, depends on the ecological niche of probiotics within the gut.[16–18] Inter-individual variability in microbiota composition poses a major translational barrier. While gut microbes clearly influence seizure activity, the relevance of compositional and functional changes remains uncertain, as most insights stem from animal studies. Elucidating how microbiota-driven neural signals—especially those conveyed via the vagus nerve—impact brain function may uncover novel therapeutic pathways.

The brain's cholinergic system regulates neuronal excitability and synaptic plasticity through acetylcholine receptor (AChR) subtypes[19,20] and plays a key role in epilepsy.[21] A medial septum-hippocampus cholinergic circuit has been shown to suppress seizures in both animal models and patients.[22] Intestinal cholinergic signaling is equally critical, with cholinergic

Please cite this article in press as: Jia et al., Gut-brain cholinergic signaling mediates the antiseizure effects of *Bacteroides fragilis*, Neuron (2025), https://doi.org/10.1016/j.neuron.2025.11.029

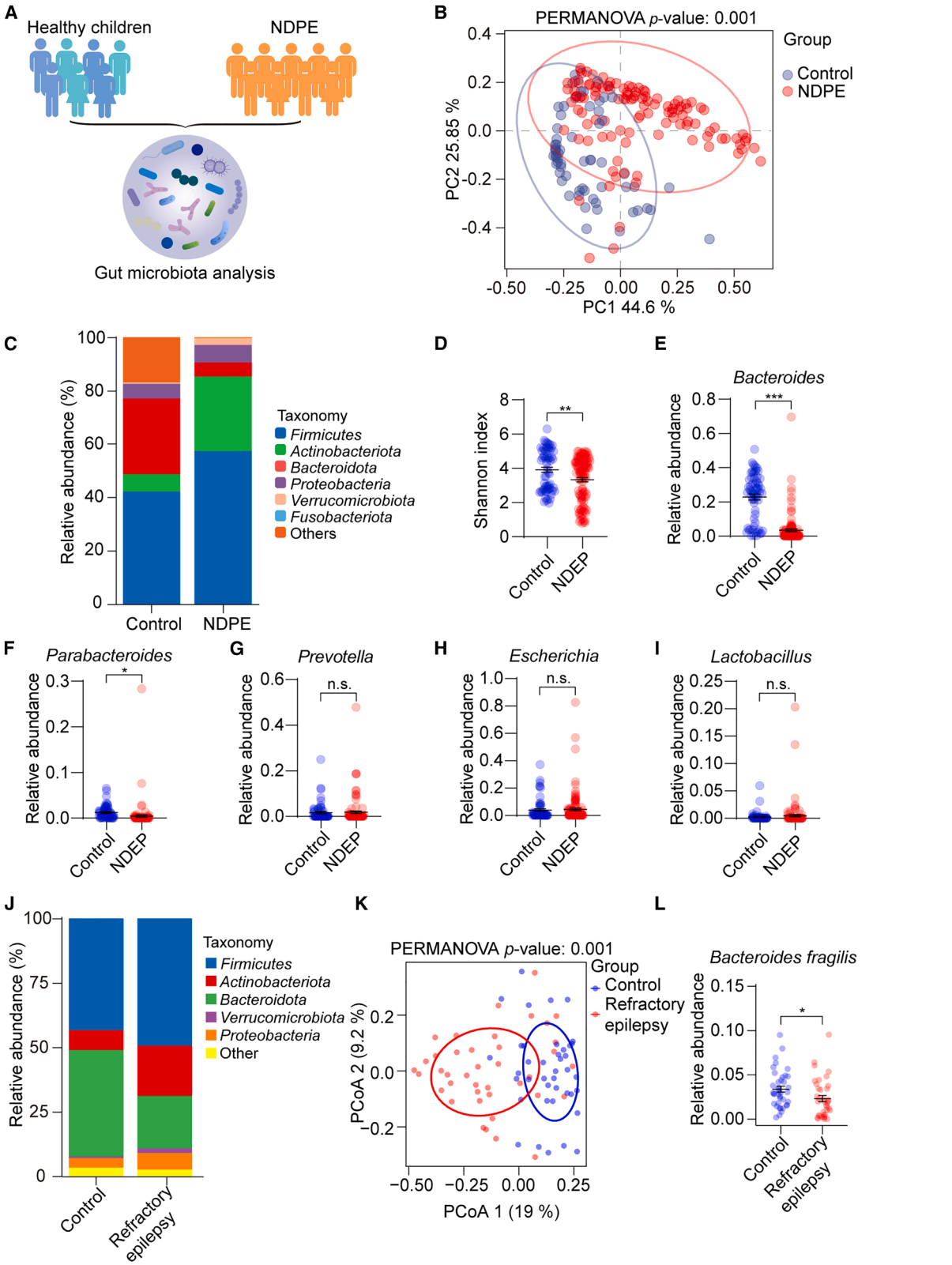

(legend on next page)

Please cite this article in press as: Jia et al., Gut-brain cholinergic signaling mediates the antiseizure effects of *Bacteroides fragilis*, Neuron (2025), https://doi.org/10.1016/j.neuron.2025.11.029

neurons activating calcium currents in epithelial cells to maintain gut homeostasis, and gut microbes modulate host behavior via excitatory cholinergic pathways.[23,24] These findings imply that gut-microbiota-mediated cholinergic pathways may modulate neural activity relevant to epilepsy via gut-brain communication.

This study aims to elucidate the mechanisms through which the microbiome-gut-brain axis mediates probiotic-induced seizure suppression.[25,26] Using pentylenetetrazole (PTZ)- and kainic-acid (KA)-induced seizure models[27,28] in combination with clinical investigation, we demonstrate that *Bacteroides fragilis* (*B. fragilis*) exerts antiseizure effects by enhancing vagus-nerve-mediated cholinergic gut-brain signaling, an effect supported by a defined colonic choline acetyltransferase-positive ($ChAT^+$) neuronal circuit. Its therapeutic efficacy is further shaped by ecological interactions with *Lactobacillus* and validated in children with refractory epilepsy.

RESULTS

Reduced fecal abundance of *B. fragilis* in pediatric epilepsy

Previous research has demonstrated that individuals with epilepsy experience alterations in gut microbiota composition, suggesting that therapeutic strategies targeting the microbiota may hold promise for epilepsy treatment.[14,29] To explore the shifts in intestinal microbiota in children with epilepsy, we performed 16S rRNA gene sequencing on fecal samples from 114 patients with newly diagnosed pediatric epilepsy (NDPE) and 63 healthy controls (Figure 1A; Tables S1 and S2). Significant differences in gut microbiota composition were observed between the NDPE and control groups (Figures 1B and 1C), with the NDPE group showing reduced alpha diversity compared with controls (NDPE: 3.333 ± 0.12 vs. control: 3.91 ± 0.15; $p = 0.004$) (Figure 1D). Notably, the abundance of *Bacteroides* in the NDPE group was significantly lower than that of the healthy controls (NDPE: 0.034 ± 0.008 vs. control: 0.23 ± 0.017, $p < 0.001$) at the genus level (Figure 1E). While other genera, such as *Escherichia* (NDPE: 0.045 ± 0.01 vs. control: 0.04 ± 0.01; $p = 0.7679$), *Prevotella* (NDPE: 0.018 ± 0.006 vs. control: 0.017 ± 0.005; $p = 0.9013$), and *Lactobacillus* (NDPE: 0.005 ± 0.002 vs. control: 0.0025 ± 0.001; $p = 0.4092$), showed no significant differences, the levels of *Parabacteroides* were notably higher in the control group (NDPE: 0.0045 ± 0.0026 vs. control: 0.012 ± 0.0017, $p = 0.0343$) (Figures 1F–1I).

To validate the taxonomic profiles identified by 16S rRNA gene sequencing in NDPE and to further assess microbial alterations in children with drug-resistant epilepsy, we performed metagenomic sequencing on fecal samples from healthy controls ($n = 39$) and children with refractory epilepsy ($n = 37$) (Table S3). Consistent with the 16S rRNA gene sequencing results, metagenomic analysis revealed significant alterations in gut microbial composition between the two groups (Figures 1J and 1K). Notably, the abundance of *B. fragilis* was significantly reduced in the epilepsy group (0.023 ± 0.004) compared with controls (0.033 ± 0.003; $p = 0.032$; Figure 1L). No statistically significant differences were observed in the relative abundance of most other detected *Bacteroides* or *Lactobacillus* species between the two groups (Figures S1A and S1B). These findings suggest a potential association between gut microbiota alterations—particularly the reduced abundance of *B. fragilis*—and pediatric epilepsy, consistent with previous research. This observation underscores the need for further studies to elucidate the underlying gut-brain-axis-mediated mechanisms. In particular, the reduction in the levels of *B. fragilis* in children with refractory epilepsy provided an indication for interventions targeting the gut microbiota in pediatric epilepsy.

Antiseizure effect of *B. fragilis* in mice

Given the potential contribution of reduced *Bacteroides* abundance to epilepsy onset, restoring gut microbiota balance in pediatric patients with epilepsy through the introduction of *Bacteroides* may influence disease progression. To examine the antiseizure effects of *Bacteroides*, we administered a commercially available probiotic containing *B. fragilis* (BF839) to PTZ-induced epileptic mice. BF839 is a non-toxic strain isolated from healthy infant feces under anaerobic conditions.[30,31] Recent studies have highlighted the association between non-toxigenic *B. fragilis* and immune system modulation, suggesting that specific strains could serve as potential probiotics to alleviate gut microbial imbalances.[32,33] Therefore, we initially tested the potential of BF839 as a treatment for pediatric epilepsy in a mouse model.

Figure 1. Alterations in the fecal microbiota composition of pediatric epilepsy patients, including newly diagnosed and refractory cases

(A) Diagram of the experimental methods.

(B) PCoA of gut microbiota composition at the genus level, based on the weighted UniFrac matrix, comparing healthy children and NDPE patients. Shapes and colors of the spots represent individual samples. Colored ellipses denote the 95% confidence interval (CI) ranges within the healthy children and NDPE patients.

(C) Relative abundance of gut bacterial phyla in healthy children ($n = 63$) and NDPE patients ($n = 114$).

(D) Shannon α-diversity index of the gut microbiota (unpaired *t* test).

(E) Relative abundance of *Bacteroides* (unpaired *t* test).

(F) Relative abundance of *Parabacteroides* (unpaired *t* test).

(G) Relative abundance of *Prevotella* (unpaired *t* test).

(H) Relative abundance of *Escherichia* (unpaired *t* test).

(I) Relative abundance of *Lactobacillus* (unpaired *t* test).

(J) Metagenomic sequencing analysis of gut bacterial phyla in healthy children ($n = 39$) and patients with refractory epilepsy ($n = 37$). Relative abundances are shown for each group.

(K) PCoA of gut microbiota composition at the genus level, based on the weighted UniFrac distance. Each point represents an individual sample; shapes and colors distinguish healthy and refractory epilepsy groups. Colored ellipses indicate 95% CIs.

(L) Relative abundance of *B. fragilis* (unpaired *t* test).

Data are presented as mean ± SEM.

See also Figure S1, Tables S1, S2, and S3, and Data S1 and S2.

Please cite this article in press as: Jia et al., Gut-brain cholinergic signaling mediates the antiseizure effects of *Bacteroides fragilis*, Neuron (2025), https://doi.org/10.1016/j.neuron.2025.11.029

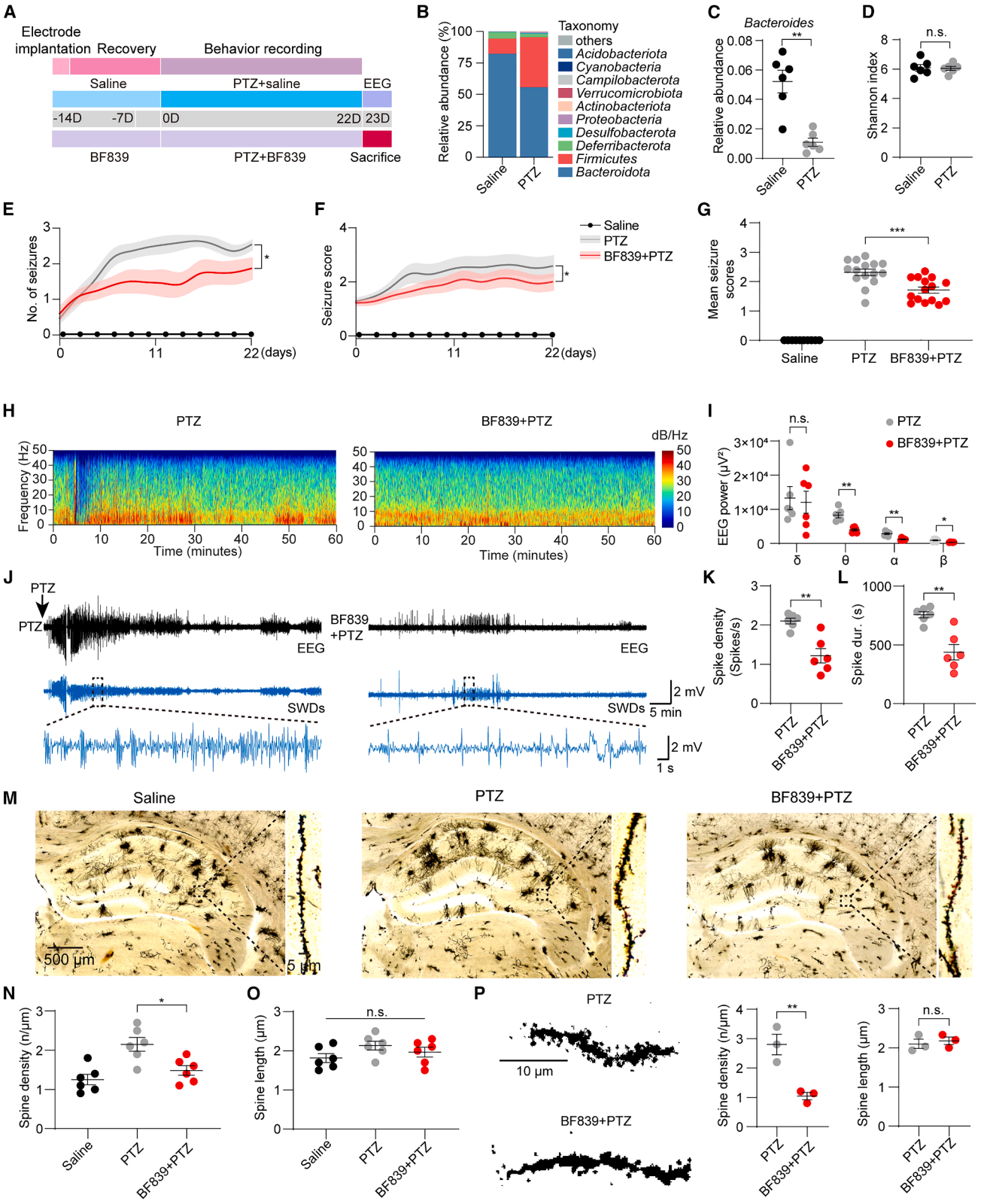

(legend on next page)

Please cite this article in press as: Jia et al., Gut-brain cholinergic signaling mediates the antiseizure effects of *Bacteroides fragilis*, Neuron (2025), https://doi.org/10.1016/j.neuron.2025.11.029

The PTZ-induced seizure model, known for its resistance to several antiseizure medication, has been widely employed for the evaluation of novel anticonvulsants.[28,34] In this study, male C57BL/6 juvenile mice (4 weeks old) were administered BF839 via oral gavage (1×10^9 colony-forming unit [CFU]/day) for 7 days prior to PTZ-induced seizures (Figure 2A). Analysis of the gut microbiota revealed that *Bacteroidota* and *Firmicutes* were the most dominant phyla in both the saline and PTZ groups (Figure 2B). A significant reduction in *Bacteroides* abundance was observed in the fecal samples of PTZ-treated mice, compared with those in the saline group (saline: 0.052 ± 0.007 vs. PTZ: 0.011 ± 0.003; $p = 0.0021$) (Figure 2C). Statistical analysis revealed no significant differences in the Shannon index between the treatment groups (saline: 6.09 ± 0.23 vs. PTZ: 6.05 ± 0.13; $p = 0.8879$) (Figure 2D). Subsequent quantification of chronic spontaneous convulsive seizures showed that, compared with the mice in the PTZ group, the mice treated with BF839 showed a significant reduction in seizure frequency starting from day 3 after PTZ injection (Figure 2E). Video analysis further revealed that seizure severity gradually increased in the PTZ group, while it decreased and stabilized in BF839-treated mice after the 4th day of PTZ injection (Figure 2F). The mean seizure score in the BF839 + PTZ group was significantly lower than in the PTZ group (BF839 + PTZ: 1.71 ± 0.10 vs. PTZ: 2.32 ± 0.11; $p < 0.001$) (Figure 2G).

In the PTZ-induced kindling model, which simulates refractory temporal lobe epilepsy characterized by abnormal hippocampal discharges, electroencephalography (EEG) was employed to assess the effects of BF839 on hippocampal hyperexcitation.[35] Representative EEG patterns in the hippocampus during seizures are shown in Figure 2H, with corresponding spectral analyses presented in Figure 2I. BF839 treatment significantly reduced the power spectral density of theta (PTZ: 8,262.89 ± 742.69 μV^2 vs. BF839 + PTZ: 3,983.34 ± 327.44 μV^2; $p = 0.0022$), alpha (PTZ: 2,892.20 ± 250.90 μV^2 vs. BF839 + PTZ: 1,229.80 ± 138.14 μV^2; $p = 0.0022$), and beta (PTZ: 918.74 ± 149.55 μV^2 vs. BF839 + PTZ: 361.17 ± 36.85 μV^2; $p = 0.0087$) waves while having no significant effect on delta (PTZ: 13,299.31 ± 3,398.75 μV^2 vs. BF839 + PTZ: 12,082.84 ± 3,212.86 μV^2; $p = 0.8182$) wave activity. We further focused on spike-wave discharges (SWDs), a key electrophysiological hallmark of epileptic seizures characterized by synchronized neuronal hyperactivity (Figure 2J).[36] Compared with the PTZ-induced untreated group, BF839-treated mice exhibited statistically significant reductions in both SWD spike density (PTZ: 2.11 ± 0.07 vs. BF839 + PTZ: 1.22 ± 0.18; $p = 0.0043$) (Figure 2K) and spike duration (PTZ: 757.85 ± 26.56 s vs. BF839 + PTZ: 438.067 ± 65.40 s; $p = 0.0043$) (Figure 2L), indicating a marked attenuation of ictal discharge intensity. Overexcitability of hippocampal neurons is often accompanied by morphological abnormalities in dendritic spines.[37] To investigate this, Golgi staining was used to evaluate dendritic spine density, revealing a significant decrease in spine density in BF839-treated mice compared with the PTZ group, with no observed changes in spine length (Figures 2M–2O). These outcomes were further confirmed using recombinant adeno-associated virus (rAAV)-non-cell-type-specific sparse (NCSP)-YFP-2E5 virus labeling of hippocampal dentate gyrus (DG) neurons, where BF839 treatment similarly reduced dendritic spine density (PTZ: 2.80 ± 0.346 vs. BF839 + PTZ: 1.04 ± 0.124; $p = 0.0088$) without affecting spine length (PTZ: 2.10 ± 0.12 vs. BF839 + PTZ: 2.17 ± 0.097; $p = 0.6408$) (Figure 2P). Given the link between dendritic structural abnormalities and the development of spontaneous recurrent seizures, this result determined the effect of BF839 on hippocampal spine-dendritic remodeling in PTZ-induced seizure mice, also suggesting a gut-brain axis mechanism underlying its antiseizure effect.

To evaluate the modulatory effect of BF839 during PTZ-induced epileptogenesis, we administered BF839 concurrently with PTZ kindling for 22 consecutive days and monitored seizure outcomes longitudinally to determine the onset of its anticonvulsant effect (Figure S2A). Notably, BF839-treated mice exhibited an earlier reduction in seizure severity (day 12: PTZ: 2.65 ± 0.36 vs. BF839 + PTZ: 1.79 ± 0.24; $p = 0.033$) followed by a later decrease in seizure frequency (day 14: PTZ: 3.00 ± 0.00 vs. BF839 + PTZ: 2.00 ± 0.26; $p = 0.012$) compared with the PTZ-only group, indicating a progressive inhibitory action during epileptogenesis. Quantitative analyses further confirmed that BF839 significantly reduced the seizure frequency (PTZ: 2.28 ± 0.06 vs. BF839 + PTZ: 1.92 ± 0.06; $p = 0.0022$) and

Figure 2. BF839 reduces PTZ-induced seizures and regulates synaptic activity of hippocampal neurons

(A) Experimental procedure timeline.
(B) Relative abundance of gut bacterial phyla in saline-treated mice ($n = 6$) and PTZ-induced epileptic mice ($n = 6$/group).
(C) Relative abundance of *Bacteroides* ($n = 6$/group) (Welch's *t* test).
(D) Shannon α-diversity index of gut microbiota in grouped data ($n = 6$/group) (Welch's *t* test).
(E) Number (no.) of seizures per animal per day in each group following PTZ injections (Mann-Whitney test, $^*p < 0.05$).
(F) Mean seizure score per day for each animal after PTZ injections (Mann-Whitney test).
(G) Mean seizure scores per day across 12 PTZ injections for each animal (saline, $n = 6$; PTZ and BF839, $n = 15$) (unpaired *t* test).
(H) Representative EEG traces and power spectrograms recorded from the hippocampus during seizures in PTZ and BF839 + PTZ groups.
(I) Spectral analysis of hippocampal EEGs during seizures ($n = 6$/group) (Mann-Whitney test).
(J) Representative EEG recordings from mice in the PTZ and BF839 + PTZ groups following PTZ injection. Blue traces indicate SWDs.
(K) Quantification of spike density in PTZ and BF839 + PTZ groups ($n = 6$/group) (Mann-Whitney test).
(L) Comparison of spike duration during EEG recordings between PTZ and BF839 + PTZ groups ($n = 6$/group) (Mann-Whitney test).
(M–O) Golgi-stained images of hippocampal dendrites and dendritic spines (M), with quantified spine density (N) and length (O) ($n = 10$ fields from 6 mice per group).
(P) Representative images of hippocampal neurons labeled with rAAV-NCSP-YFP-2E5, showing average spine density and spine length per dendritic segment ($n = 3$/group) (Mann-Whitney test).
Data are presented as mean ± SEM, n.s., not significant, $^*p < 0.05$, $^{**}p < 0.01$, $^{***}p < 0.001$.
See also Figures S2 and S3.

Please cite this article in press as: Jia et al., Gut-brain cholinergic signaling mediates the antiseizure effects of *Bacteroides fragilis*, Neuron (2025), https://doi.org/10.1016/j.neuron.2025.11.029

decreased the severity scores per seizure (PTZ: 2.53 ± 0.071 vs. BF839 + PTZ: 1.91 ± 0.045; p = 0.0022) in PTZ group (Figures S2B and S2C). Representative hippocampal EEG recordings during seizures (Figure S2D), together with spectral analyses (Figure S2E), demonstrated that BF839 co-administration markedly suppressed the power spectral density of theta (PTZ: 7,995.99 ± 129.84 μV^2 vs. BF839 + PTZ: 3,947.50 ± 118.28 μV^2; p = 0.0022), alpha (PTZ: 2,666.61 ± 129.56 μV^2 vs. BF839 + PTZ: 1,468.60 ± 31.91 μV^2; p = 0.0022), and beta (PTZ: 952.93 ± 49.57 μV^2 vs. BF839 + PTZ: 383.99 ± 30.78 μV^2; p = 0.0022) oscillations. Furthermore, BF839 treatment significantly reduced both the spike density (PTZ: 1.99 ± 0.12 vs. BF839 + PTZ: 0.94 ± 0.068; p = 0.0022) and the duration (PTZ: 715.47 ± 43.32 s vs. BF839 + PTZ: 338.80 ± 24.45 s; p = 0.0022) of SWDs compared with the PTZ group (Figures S2F and S2G). Collectively, these findings demonstrate that BF839 exerts progressive anticonvulsant effects during PTZ-induced epileptogenesis, first alleviating seizure severity and subsequently reducing seizure frequency. The combined behavioral and electrophysiological improvements suggest that sustained BF839 administration stabilizes neural excitability and may act through cumulative gut-brain-axis-mediated mechanisms to confer seizure protection.

To further validate the sustained inhibitory effects of BF839 in chronic epilepsy, we employed a KA-induced status epilepticus mouse model (Figure S3A). BF839 treatment significantly reduced seizure duration (KA: 306.67 ± 15.58 vs. KA + BF839: 241.33 ± 21.04; p = 0.041) and daily seizure frequency (KA: 2.67 ± 0.21 vs. KA + BF839: 1.50 ± 0.22; p = 0.026) at 12–14 days post-induction (Figure S3B). Moreover, these anticonvulsant effects persisted, as BF839-treated mice maintained significantly shorter seizure duration (KA: 380.67 ± 15.47 vs. KA + BF839: 231.83 ± 17.38; p = 0.0043) and lower daily seizure frequency (KA: 3.00 ± 0.26 vs. KA + BF839: 1.33 ± 0.21; p = 0.0065) at 23–25 days post-induction compared with the KA group (Figure S3C). Representative hippocampal EEG recordings during seizures are shown in Figure S3D, with corresponding spectral analyses in Figure S3E. BF839 treatment robustly suppressed the power spectral density across delta (KA: 10,720.71 ± 490.32 vs. KA + BF839: 6,930.12 ± 428.65 μV^2; p = 0.0022), theta (KA: 8,005.36 ± 501.38 vs. KA + BF839: 3,609.97 ± 188.99 μV^2; p = 0.0022), alpha (KA: 2,710.22 ± 121.86 vs. KA + BF839: 1,424.93 ± 63.55 μV^2; p = 0.0022), and beta (KA: 860.92 ± 73.62 vs. KA + BF839: 338.57 ± 30.42 μV^2; p = 0.0022) frequency bands. Compared with KA-only mice, BF839 administration markedly reduced SWD spike density (KA: 1.83 ± 0.046 vs. KA + BF839: 0.87 ± 0.07; p = 0.0022) and shortened spike duration (KA: 362.50 ± 12.95 vs. KA + BF839: 231.83 ± 20.02 s; p = 0.0043) (Figures S3F–S3H), indicating attenuated ictal discharge intensity. To assess the cellular correlates of BF839-mediated neuromodulation, we examined c-Fos immunoreactivity as a marker of neuronal activation. KA challenge induced pronounced c-Fos expression in hippocampal CA3 (control: 32.67 ± 2.46; KA: 87.33 ± 3.08; KA + BF839: 43.67 ± 4.28; $p_{\text{control-KA}} < 0.001$; $p_{\text{KA-(KA + BF839)}} < 0.001$) and DG regions (control: 27.50 ± 2.86; KA: 59.83 ± 3.26; KA + BF839: 38.67 ± 2.19; $p < 0.001$ for both comparisons), but not in CA1 (control: 117.67 ± 4.22; KA: 131.33 ± 6.01; KA + BF839: 118.67 ± 3.36; $p_{\text{control-KA}}$ = 0.129; $p_{\text{KA-(KA + BF839)}}$ = 0.167) (Figures S3I–S3L). Collectively, these results demonstrate that BF839 confers robust and sustained protection in multiple models of chronic epilepsy.

To explore the role of BF839 in reducing seizures and determine whether enhancing its ecological niche within the gut can amplify its antiseizure effects, antibiotics (ABXs) including vancomycin, streptomycin, neomycin, and gentamicin were administered for 3 days to deplete the gut microbiota.[38] This was followed by 11 days of intragastric BF839 treatment, which continued until the end of the experiment, in conjunction with PTZ-induced seizures (Figure S4A). After the eradication of bacteria by ABX, the number of daily seizures in the ABX group decreased compared with the PTZ group, although the reduction was not statistically significant (Figure S4B). However, mice receiving BF839 treatment following ABX pretreatment exhibited a significantly greater reduction in daily seizure frequency compared with both the PTZ and BF839 groups (Figure S4B). Specifically, the mean number of seizures (ABX + BF839 + PTZ: 0.68 ± 0.085 vs. BF839 + PTZ: 1.29 ± 0.16; p = 0.0045) and seizure duration time (ABX + BF839 + PTZ: 332.78 ± 36.74 vs. BF839 + PTZ: 464.67 ± 42.51 s; $p < 0.001$) in the BF839 post-ABX group was significantly lower than in the BF839 group alone (Figures S4C and S4D). However, there was no significant difference in seizure latency between the ABX + BF839 + PTZ group and the BF839 + PTZ group (696.30 ± 55.76 vs. 494.90 ± 59.86 s; p = 0.1008) (Figure S4E). Additionally, the BF839 post-ABX group showed a lower seizure score compared with the BF839 group (ABX + BF839 + PTZ: 1.29 ± 0.059 vs. BF839 + PTZ: 1.62 ± 0.08; p = 0.0028) (Figures S4F and S4G). BF839 gavage had no significant effect on body weight in the mice (Figure S4H). In summary, these findings indicate that intragastric administration of *B. fragilis* reduces seizure susceptibility and ameliorates hippocampal neuronal hyperexcitability in epilepsy models, as supported by EEG spectral features and restoration of dendritic spine morphology.

Antiseizure effects of BF839 mediated by the vagal gut-brain neural signals

The vagus nerve plays a critical role in relaying metabolic signals between the gastrointestinal tract and the brain.[39] Given that vagus nerve stimulation (VNS) is a common clinical intervention for refractory epilepsy, this highlights the strong connection between vagus nerve activity and epilepsy.[40–42] To verify the potential role of vagus nerve activity in the antiseizure effects mediated by the gut-brain axis through BF839, spontaneous vagal nerve activity was recorded in awake mice through vagus nerve electroneurogram recording (Figure 3A).[43] To avoid movement interference, vagal ganglion activity was also recorded and measured in anesthetized mice during mechanical stimulation and intraluminal perfusion of BF839 in the colon (Figures S4I–S4K). Vagal nerve activities were recorded across all experimental groups prior to PTZ injection using the Apollo noise reduction system (Figure 3A). The vagal nerve activity is illustrated in Figure 3B, with firing rate analysis showing that BF839 treatment significantly enhanced vagal nerve activity compared with the saline (BF839 + PTZ: 24.23 ± 2.50 vs. saline: 8.39 ± 0.89; $p < 0.001$) and PTZ (BF839 + PTZ: 24.23 ± 2.50 vs.

Please cite this article in press as: Jia et al., Gut-brain cholinergic signaling mediates the antiseizure effects of *Bacteroides fragilis*, Neuron (2025), https://doi.org/10.1016/j.neuron.2025.11.029

CellPress

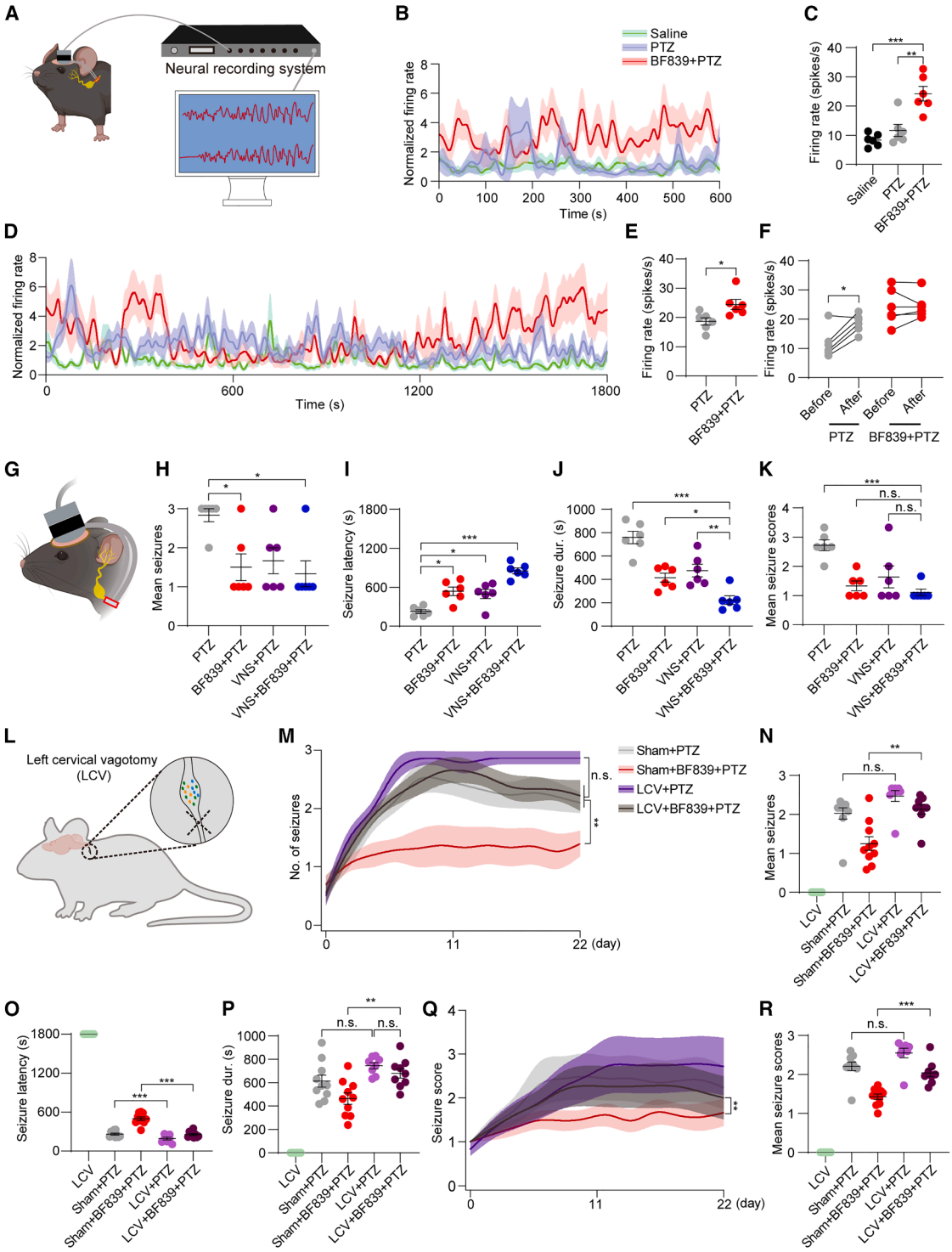

Figure 3. BF839 enhances the antiseizure effect of VNS by activating the cervical NG, while unilateral vagotomy reduces its therapeutic effect

(A) Schematic diagram of experimental mice showing electroneurogram recording from the left vagus nerve.

(B) Electroneurogram recording of the left vagus nerve prior to the 12th PTZ injection (normalized average vagal firing rate compared with saline).

(C) Analysis of vagus nerve firing rate from electroneurogram recordings before PTZ injection (n = 6/group) (ordinary one-way ANOVA).

(D) Electroneurogram recording of vagus nerve activity during seizures.

(E) Analysis of vagus nerve firing rate during seizures (n = 6/group) (Mann-Whitney test).

(legend continued on next page)

Please cite this article in press as: Jia et al., Gut-brain cholinergic signaling mediates the antiseizure effects of *Bacteroides fragilis*, Neuron (2025), https://doi.org/10.1016/j.neuron.2025.11.029

PTZ: 11.71 ± 2.04; p = 0.001) groups (Figure 3C). After PTZ injection, BF839-treated mice continued to exhibit higher neural activity in the nodose (vagal) ganglia compared with the PTZ group (BF839 + PTZ: 24.47 ± 1.71 vs. PTZ: 18.66 ± 1.26; p = 0.026) (Figures 3D and 3E).

A comparison of vagal nerve activity pre- and post-PTZ injection within each group revealed a significant increase in the PTZ group, whereas the BF839 group showed a more moderate elevation, indicating that BF839 enhances vagal nerve activity, though this effect may plateau at a certain threshold (Figure 3F). To further elucidate the role of the vagus nerve in seizure attenuation, micro-cuff electrodes were used to stimulate the vagal ganglia following PTZ injection, as described in a prior study (Figure 3G).[44] At the final PTZ injection, mice in the BF839 + PTZ (1.50 ± 0.34; p = 0.0258) and VNS + BF839 + PTZ (1.33 ± 0.33; p = 0.011) groups exhibited significantly fewer seizures compared with the PTZ group (2.83 ± 0.17) (Figure 3H). However, VNS alone did not result in a significant reduction in seizure numbers compared with the PTZ group (VNS + PTZ: 1.67 ± 0.33 vs. PTZ: 2.83 ± 0.17; p = 0.0581) (Figure 3H). The latency to seizure onset was significantly increased in the BF839 + PTZ (537.00 ± 65.69 s; p = 0.039), VNS + PTZ (495.83 ± 71.08 s; p = 0.0128), and VNS + BF839 + PTZ (853 ± 45.34 s; p < 0.001) groups compared with the PTZ group (226.50 ± 29.25 s) (Figure 3I), with the combination of VNS and BF839 showing the most prolonged seizure onset. Similarly, the VNS + BF839 + PTZ group (223.67 ± 36.90 s) exhibited a shorter seizure duration compared with the PTZ (759.50 ± 53.67 s; p < 0.001), BF839 + PTZ (415.17 ± 38.11 s; p = 0.0381), and VNS + PTZ (476.17 ± 53.34 s; p = 0.0049) groups (Figure 3J). Furthermore, the VNS + BF839 + PTZ group showed a significantly lower mean seizure score compared with the PTZ group (VNS + BF839 + PTZ: 1.11 ± 0.11 vs. PTZ: 2.72 ± 0.18; p < 0.001), although no marked differences were found when compared with the BF839 + PTZ (1.33 ± 0.17; p = 0.9039) and VNS + PTZ (1.42 ± 0.20; p = 0.3946) groups (Figure 3K). These findings indicate that while acute VNS alone exerted limited efficacy, its combination with BF839 produced a synergistic antiseizure effect, underscoring the promise of personalized probiotic-neural interventions optimized to individual vagal responsiveness and microbial colonization capacity in refractory epilepsy.

To further validate the role of VNS in the seizure-suppressive effects of BF839, we examined the effect of BF839 on seizure severity in PTZ-induced mice following left cervical vagotomy (LCV). This procedure, involving the resection and cauterization of all afferent and efferent left cervical vagal fibers, effectively eliminated vagal neurotransmission (Figure 3L). Results demonstrated that LCV significantly increased the number of seizures in BF839-treated mice compared with those without LCV (LCV: 2.13 ± 0.12 vs. non-LCV: 1.25 ± 0.18; p = 0.0027) (Figures 3M and 3N). However, PTZ-induced mice with and without LCV had comparable seizure frequencies (LCV: 2.47 ± 0.14 vs. non-LCV: 2.03 ± 0.15; p = 0.2438) (Figures 3M and 3N). Seizure latency was also shortened in both BF839-treated (253.67 ± 15.57 s; p < 0.001) and PTZ-induced (194.50 ± 21.03 s; p = 0.018) mice post-LCV compared with those without LCV (498.20 ± 27.72 s) (Figure 3O). In contrast, seizure duration was prolonged in BF839-treated mice after LCV (680.11 ± 40.97 s) relative to BF839-only treated mice (463.9 ± 48.76 s; p = 0.0083), with no significant difference in duration between LCV (746.00 ± 26.72 s; p = 0.196) and non-LCV (613.80 ± 52.08 s; p = 0.756) PTZ-induced mice (Figure 3P). LCV also exacerbated seizure severity in the BF839 + PTZ group (LCV: 2.04 ± 0.10 vs. non-LCV: 1.42 ± 0.07; p < 0.001), while no significant difference in seizure severity was observed in the PTZ group (LCV: 2.55 ± 0.12 vs. non-LCV: 2.21 ± 0.11; p = 0.0977) (Figures 3Q and 3R). These results demonstrate that LCV significantly attenuates the anticonvulsant effects of BF839, highlighting the vagus nerve's critical role in the gut-brain signaling pathway mediated by BF839.

BF839 enhances the gut-brain ACh signaling

Based on the above results that demonstrate the crucial role of neural pathways in the gut-brain axis mechanism of BF839's antiseizure effect, we next performed targeted metabolomic profiling of neurotransmitters and neuromodulators in colonic tissues to identify probiotic-dependent neuroactive metabolites potentially associated with seizure modulation. Forty neuroactive compounds were quantified, revealing significant differences between the PTZ and BF839-treated groups (Figure 4A). Notable alterations in choline metabolites were observed, suggesting that the effects of BF839 may involve modulation of cholinergic neurotransmission in the colon (Figures 4A and 4B). Other neurotransmitters linked to epilepsy, such as 4-aminobutyric acid (GABA) (PTZ: 1.00 ± 0.09 vs. BF839: 1.50 ± 0.19; p = 0.132) and glutamine (PTZ: 1.00 ± 0.18 vs. BF839 + PTZ: 0.71 ± 0.06; p = 0.309), showed no significant differences (Figures S5A and

(F) Comparison of vagus nerve firing rates before and after PTZ injection in mice with and without BF839 treatment (n = 6/group) (Mann-Whitney test).
(G) Schematic diagram of experimental mice with VNS.
(H) Mean number of seizures observed during the last PTZ injection for each group (n = 6/group) (ordinary one-way ANOVA).
(I) Seizure latency at the last PTZ injection (n = 6/group) (ordinary one-way ANOVA).
(J) Seizure duration (dur.) at the last PTZ injection (n = 6/group) (ordinary one-way ANOVA).
(K) Mean seizure score during the last PTZ injection for each group (n = 6/group) (ordinary one-way ANOVA).
(L) Schematic representation of an experimental mouse with LCV.
(M) Number of seizures per animal per day in each group following PTZ injections (ordinary one-way ANOVA).
(N) Mean number of seizures per animal per day after PTZ injections (n = 8–10/group) (ordinary one-way ANOVA).
(O) Seizure latency at the last PTZ injection (n = 8–10/group) (ordinary one-way ANOVA).
(P) Seizure duration at the last PTZ injection (n = 8–10/group) (ordinary one-way ANOVA).
(Q) Seizure scores per day for each group following PTZ injections (*p < 0.05, ordinary one-way ANOVA).
(R) Mean seizure score per day per animal across 12 PTZ injections (n = 8–10/group) (ordinary one-way ANOVA). Data are presented as mean ± SEM.
See also Figure S4.

Please cite this article in press as: Jia et al., Gut-brain cholinergic signaling mediates the antiseizure effects of *Bacteroides fragilis*, Neuron (2025), https://doi.org/10.1016/j.neuron.2025.11.029

CellPress

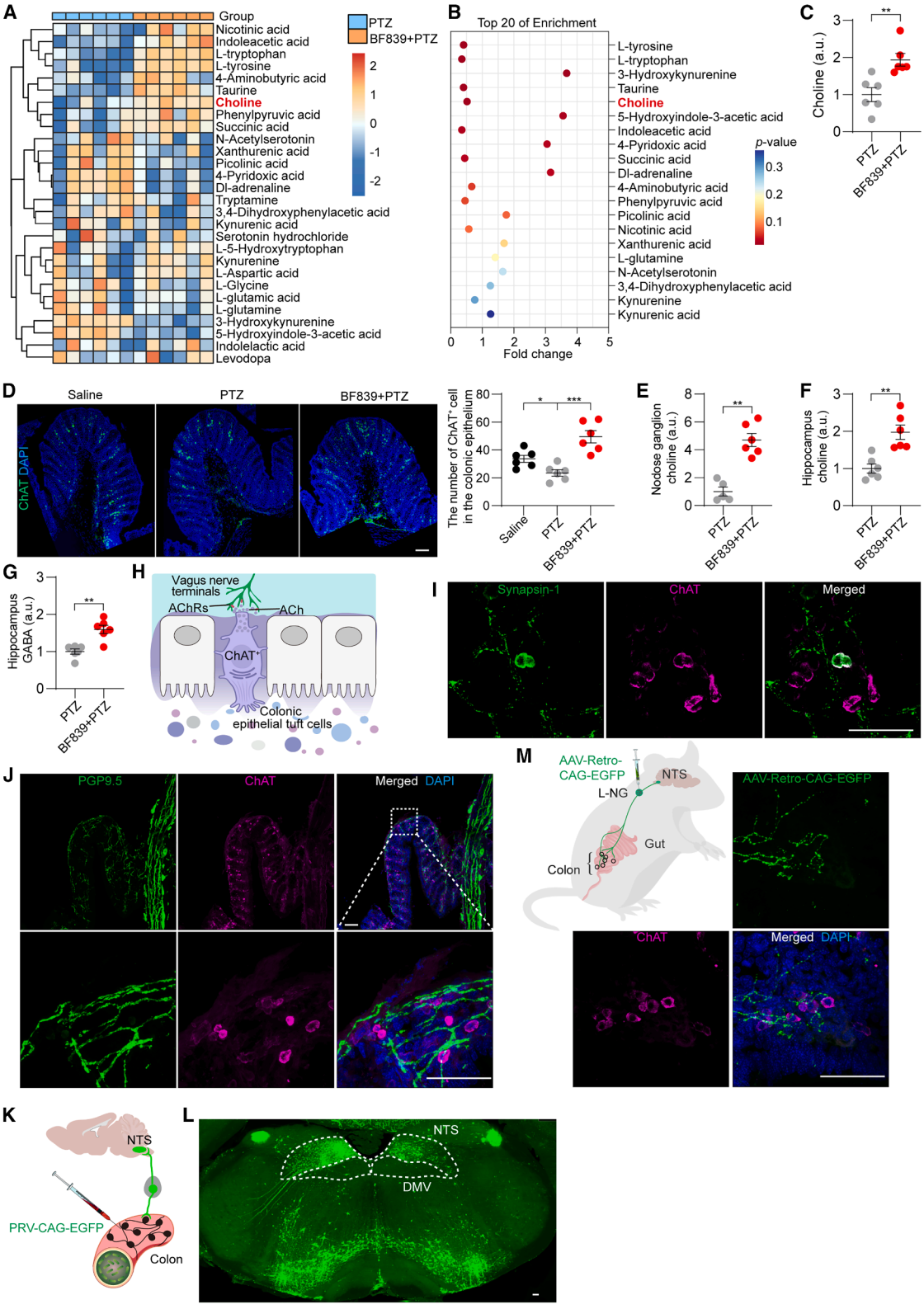

Figure 4. BF839 increases ChAT levels in the colon, NG, and hippocampus

(A) Expression levels of neurotransmitter-related metabolites in the gut of mice from the PTZ and BF839 + PTZ groups. Heatmap color scale indicates $\log_2$ fold changes relative to the PTZ group baseline, with blue denoting downregulation, orange denoting upregulation, and gray indicating minimal change.

(legend continued on next page)

Please cite this article in press as: Jia et al., Gut-brain cholinergic signaling mediates the antiseizure effects of *Bacteroides fragilis*, Neuron (2025), https://doi.org/10.1016/j.neuron.2025.11.029

S5B). It is worth noting that choline levels, which are highly associated with epilepsy and involved in the gut-brain metabolic crosstalk,[23,45,46] exhibited significant differences between the PTZ and BF839 + PTZ (PTZ: 1 ± 0.18 vs. BF839 + PTZ: 1.94 ± 0.17; $p = 0.0043$) groups (Figure 4C). Given that BF839 mediates its antiseizure effects through vagal gut-brain neural signaling, and previous studies have shown that intestinal cholinergic pathways are modulated by the gut microbiota,[23,47] we next investigated whether the colonic ChAT-mediated gut-brain axis contributes to the antiseizure effects of *B. fragilis*.

We next sought to assess how BF839 modulates intestinal ChAT signaling in the PTZ model. In our study, the number of ChAT$^+$ cells in the colon of PTZ-induced mice was significantly lower than that observed in the saline group (PTZ: 23.50 ± 2.29 vs. saline: 33.6 ± 2.52; $p = 0.04$) (Figure 4D). Notably, the administration of BF839 to PTZ-induced mice (49.50 ± 4.36; $p = 0.002$) resulted in a marked increase in ChAT$^+$ cells (Figure 4D), suggesting a modulation of intestinal ChAT metabolism in the PTZ model. Furthermore, high-performance liquid chromatography (HPLC) demonstrated elevated choline levels in the nodose ganglion (NG) of BF839-treated mice, in contrast to the PTZ group (BF839 + PTZ: 4.70 ± 0.46 vs. PTZ: 1 ± 0.32; $p = 0.0043$) (Figure 4E). Immunostaining for phosphorylated extracellular signal-regulated kinase (pERK-1), a marker of neuronal activation in the NG,[48] revealed a significantly higher proportion of activated cells in the BF839-treated group compared with both the saline (BF839 + PTZ: 0.078 ± 0.007, saline: 0.059 ± 0.004; $p = 0.0156$) and PTZ (PTZ: 0.062 ± 0.003; $p = 0.0156$) groups (Figures S5C and S5D).

Following the identification of the role of BF839 in modulating ChAT expression in the colon and vagal ganglia, subsequent analyses explored whether BF839 could influence hippocampal neuronal activity and neurotransmitter levels via the gut-brain axis. HPLC was employed to compare the expression levels of key epilepsy-related molecules in the hippocampus and sera of mice treated with PTZ alone or BF839 and PTZ. The results demonstrated that BF839 treatment led to a significant increase in choline and GABA levels in the hippocampus (choline: 1.97 ± 0.19; GABA: 1.59 ± 0.11) compared with the PTZ group (choline: 1.00 ± 0.12, $p = 0.0022$; GABA: 1.00 ± 0.07, $p = 0.0043$), with no significant changes detected in serum (Figures 4F, 4G, S5E, and S5F). These findings implicate the role of vagus nerve in mediating BF839's effects via gut-brain neural pathways.

Structural basis of colonic ChAT$^+$ cell-NG connectivity underlying BF839-mediated gut-brain signaling

To further clarify that BF839-activated neural signaling within the gut-brain axis is specifically mediated by ChAT, the capacity of ChAT$^+$ cells in the intestine to transmit signals to the brain via the vagus nerve was investigated. Although the proximal small intestine is densely innervated by the vagus nerve, as previously reported, we focused our analysis on the colon due to the pronounced microbial density gradient along the gastrointestinal tract.[49,50] The colon harbors the highest bacterial load—including abundant commensals such as *Bacteroides* and *Lactobacillus*—and serves as one of the key sites for host–microbiota interactions. This regional specificity supports a potential mechanistic link between microbial signals and vagus-nerve-mediated gut-brain communication. Consistent with this focus, fecal samples—reflective primarily of colonic luminal communities—were used for microbiota profiling.[51] We first sought to obtain a comprehensive cellular distribution profile of ChAT in mouse colonic epithelial cells by re-analyzing the published single-cell RNA sequencing dataset generated in previous work.[52,53] The data demonstrate that ChAT is predominantly expressed in colonic tuft cells, consistent with previous reports showing that these cells are specialized to sense intraluminal cues, display neuroendocrine features, and serve as a source of cholinergic output (Figures S6A and S6B).[47,54] We further identified robust expression of several AChRs, including Chrm1, Chrm2, Chrna4, Chrnb2, Chrnb3, Chrna6, Chrna5, Chrna3, and Chrnb4, in the NG neurons by re-analyzing the single-cell sequencing data of the vagal ganglion complex from the existing report (Figure S6C).[55] These data indicated that the ChAT-specific signals elicited by BF839 in the colon could be transmitted synaptically from the colonic epithelium to the vagal ganglion, which functions as a relay for gut-brain neural signals in response to BF839, although the colon was shown to have local expression of several AChRs (Figures S6D–S6H). Based on these observations, it was hypothesized that ChAT$^+$ tuft cells, similar to intestinal neuropod cells, may form synaptic connections from the colon to the vagus nerve,[56–58] enabling the transmission of colonic signals of BF839 through AChRs located on the vagus nerve (Figure 4H). Furthermore, co-labeling experiments using anti-ChAT and anti-synapsin-1 antibodies demonstrated that ChAT-expressing tuft cells were co-localized with the presynaptic protein synapsin-1 (Figure 4I), confirming the synaptic characteristics

(B) Neurotransmitter profiles identified by random forest analysis of targeted metabolomics, showing differentially expressed neurotransmitters in the colon of PTZ-treated mice with and without BF839 treatment (Mann-Whitney test).
(C) Choline levels in the colon of mice from PTZ and BF839 + PTZ groups ($n = 6$/group) (Mann-Whitney test).
(D) Representative immunofluorescence images of ChAT in the colon, along with quantification of ChAT$^+$ (green) cells ($n = 6$/group) (ordinary one-way ANOVA).
(E) Choline levels in the cervical NGs assessed using HPLC (Mann-Whitney test).
(F and G) Levels of choline (F) and GABA (G) in the hippocampus assessed using HPLC ($n = 6$/group) (Mann-Whitney test).
(H) Schematic diagram illustrating synaptic transmission in cholinergic tuft cells.
(I) Representative immunofluorescence images of ChAT$^+$ (purple) cells co-localized with the presynaptic marker synapsin-1 (green) at 63× magnification ($n = 3$ mice, 10 cells per mouse).
(J) Immunostaining and localization of ChAT$^+$ cells and PGP9.5 (a neural/nerve sheath marker) in the mouse colon ($n = 6$/group).
(K and L) PRV-CAG-EGFP was injected into the colon, with subsequent signal detection in the nucleus of the tractus solitarius (NTS).
(M) The left NG (L-NG) was injected with AAV9-Retro-CAG-EGFP and co-stained with ChAT in the colon. Scale bars represent 50 μm. DAPI was used for nuclear staining. Data are presented as mean ± SEM. DMV, dorsal motor nucleus of vagus.
See also Figures S5 and S6.

Please cite this article in press as: Jia et al., Gut-brain cholinergic signaling mediates the antiseizure effects of *Bacteroides fragilis*, Neuron (2025), https://doi.org/10.1016/j.neuron.2025.11.029

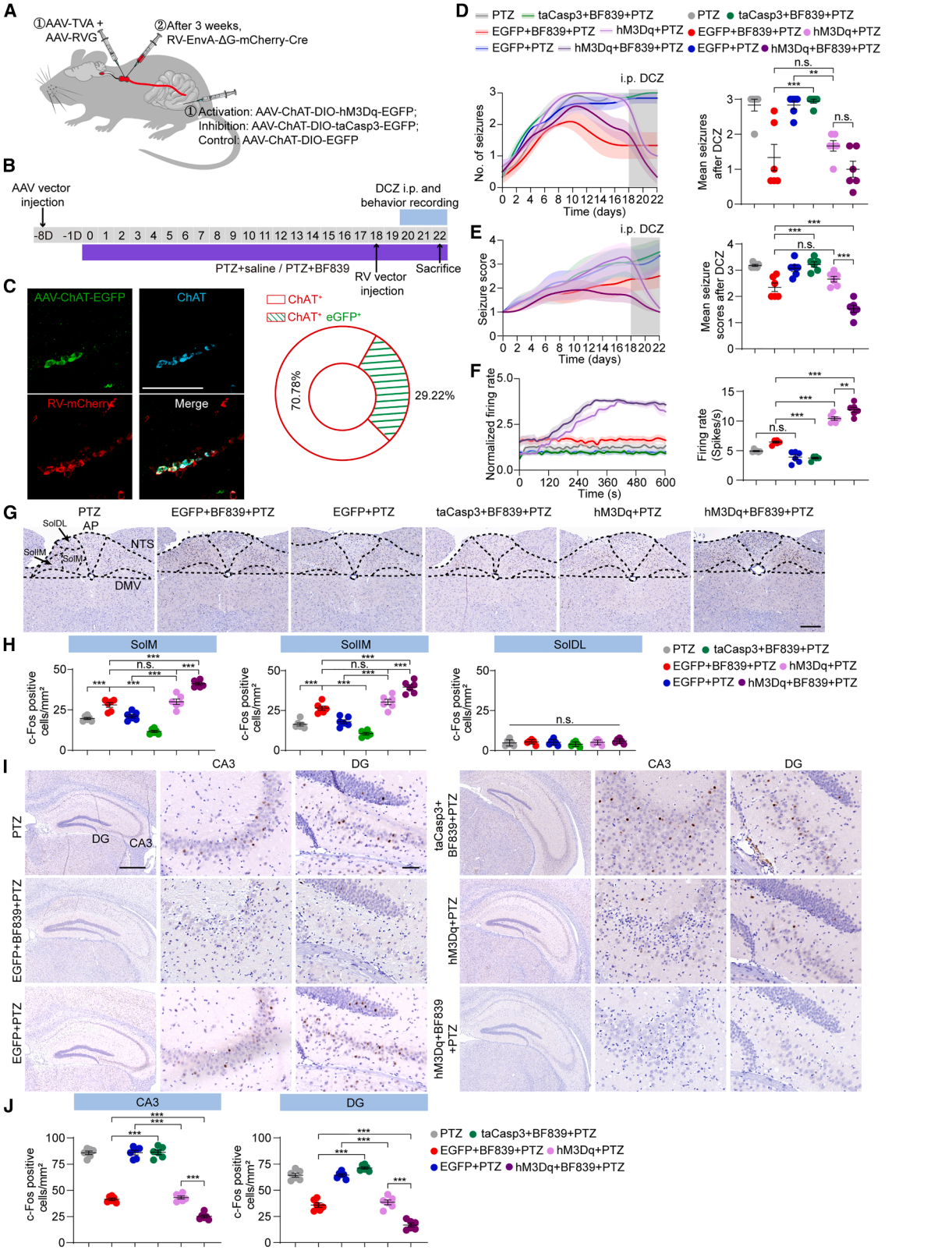

(legend on next page)

Please cite this article in press as: Jia et al., Gut-brain cholinergic signaling mediates the antiseizure effects of *Bacteroides fragilis*, Neuron (2025), https://doi.org/10.1016/j.neuron.2025.11.029

of ChAT$^+$ epithelial tuft cells in the colon. Additional co-immunostaining of the pan-neuronal marker protein gene product 9.5 (PGP9.5) and ChAT at the colonic epithelium corroborated these results (Figure 4J), suggesting that ChAT-secreting cells may detect probiotic signals and relay them to the brain via vagal transmission.

To further elucidate the gut-brain neural circuit and determine whether ChAT-expressing cells in the colon are associated with the nervous system and transmit intestinal signals to the central nervous system, we injected pseudorabies virus (PRV)-cytomegalovirus early enhancer/chicken β-actin (CAG)-EGFP into the proximal region of the colon (Figure 4K), and subsequent brain dissections were conducted to track the fluorescence signal. Our observation indicated that the PRV-CAG-EGFP signal was abundantly expressed in the nucleus tractus solitarius (NTS) (Figure 4L), confirming the neural connection between NTS and colon. This implies that probiotic-induced visceral signals from the gut can activate neurons in the NTS through the vagus nerve and efficiently travel to the brain. We further examine the potential mediation of ChAT signaling through the vagus nerve, an initial investigation focused on whether NG nerve fibers project to the colon and establish connections with ChAT$^+$ cells. To confirm this, AAV9-Retro-CAG-EGFP was injected into the NG (Figures 4M and S6I). Retrograde tracing of vagal nerve fibers labeled with AAV9-Retro-CAG-EGFP, followed by co-staining with ChAT$^+$ cells in the colon, enabled detailed three-dimensional reconstruction analysis using Imaris viewer software (Figure 4M; Video S1). This analysis revealed that vagal sensory fibers and ChAT$^+$ cells in the colon are within a short distance of each other, suggesting that NGs projecting into the colon may have established significant connections with ChAT$^+$ cells to sense and transmit a variety of stimulus signals from BF839.

Chemogenetic manipulation identifies a colonic ChAT$^+$ cell-NG circuit mediating BF839-induced seizure suppression

To directly test whether cholinergic signaling from colonic cells to NG contributes to BF839-mediated seizure protection, we employed a combinatorial viral strategy to selectively trace and manipulate the colonic ChAT$^+$-vagal afferent circuit (Figures 5A and 5B). Retrograde labeling was achieved by co-injecting RV-EnvA-ΔG-mCherry-Cre with helper viruses (AAV-hSyn-TVA and AAV-hSyn-N2cG) into the left cervical vagus trunk, while colonic ChAT$^+$ cells were transduced with either a Cre-dependent excitatory DREADD (AAV-ChAT-DIO-hM3Dq-EGFP), a pro-apoptotic construct (AAV-ChAT-DIO-taCasp3-TEVp-EGFP),[59] or a control vector (AAV-ChAT-DIO-EGFP). This approach enabled both anatomical definition and functional perturbation of the colonic ChAT$^+$ projections to the NG. By combining retrograde tracing with AAV and rabies virus (RV) vectors and ChAT immunofluorescence co-labeling, we identified co-localization between colonic ChAT$^+$ cells and retrogradely labeled NG neurons, thereby confirming a direct neural signaling pathway from colonic ChAT$^+$ cells to the NG (Figure 5C). Quantitative analysis further demonstrated that AAV-transduced neuronal somata represented 29.22% ± 7.60% of the total population of intestinal ChAT$^+$ cells (Figure 5C). Chemogenetic activation of colonic ChAT$^+$ cells in the PTZ seizure model significantly decreased seizure frequency upon deschloroclozapine (DCZ) administration (hM3Dq + PTZ: 1.67 ± 0.15 vs. EGFP + PTZ: 2.83 ± 0.11; $p = 0.005$). Conversely, ablating these neurons markedly blunted BF839's protective effect (taCasp3 + BF839 + PTZ: 2.94 ± 0.06 vs. EGFP + BF839 + PTZ: 1.33 ± 0.38; $p < 0.001$) (Figure 5D). While activation alone recapitulated BF839's effect, the combination of BF839 with chemogenetic activation produced a synergistic reduction in seizure severity (hM3Dq + BF839 + PTZ: 1.53 ± 0.13 vs. BF839 + PTZ: 2.35 ± 0.16; $p < 0.001$) (Figure 5E). These data establish both the sufficiency and necessity of the colonic ChAT$^+$→NG projection in mediating the antiepileptic action of BF839. Electrophysiological recordings further demonstrated that vagal firing was enhanced by either BF839 (hM3Dq + BF839 + PTZ: 11.90 ± 0.42 vs. BF839 + PTZ: 6.44 ± 0.15; $p < 0.001$) or activation of ChAT$^+$ cells (hM3Dq + BF839 + PTZ: 11.90 ± 0.42 vs. hM3Dq + PTZ: 10.42 ± 0.30; $p = 0.008$) and was most pronounced when the two interventions were combined (Figure 5F). Ablation of ChAT$^+$ cells abolished BF839-induced vagal activation (taCasp3 + BF839 + PTZ: 3.75 ± 0.14 vs. BF839 + PTZ: 6.44 ± 0.15; $p < 0.001$) (Figure 5F). To determine whether colonic neural activation or ablation per se affects baseline vagal activity, we recorded NG firing prior to PTZ and DCZ administration. The taCasp3 group exhibited a significantly reduced basal firing rate compared with controls (taCasp3: 3.57 ± 0.12 vs. control: 4.50 ± 0.24, $p = 0.023$),

Figure 5. Activation of the gut-vagal cholinergic pathway suppresses epileptic seizures and reduces hippocampal neuronal excitability

(A) Schematic of the experimental design.

(B) Experimental timeline.

(C) Retrograde viral tracing combined with ChAT immunofluorescence in colonic regions. Cre-dependent expression of ChAT-EGFP (green) and RV-EnvA-ΔG-mCherry-Cre (red) was used together with ChAT antibody fluorescence (cyan) to identify cholinergic cells and their projections. Quantitative analysis showed that AAV$^+$/ChAT$^+$ neurons accounted for 29.2% ± 7.6% of the total ChAT$^+$ population ($n = 3$ mice). Scale bars, 50 μm.

(D) Seizure frequency per animal per day (left) and mean daily seizure frequency per group (right) following 12 PTZ injections ($n = 6$/group).

(E) Seizure severity scores per day (left) and mean seizure score per group (right) following 12 PTZ injections ($n = 6$/group).

(F) Electroneurogram recordings of the left vagus nerve after DCZ injection (normalized average firing rate relative to saline) and analysis of vagal firing during seizures (ordinary one-way ANOVA).

(G) Representative NTS sections from PTZ-treated mice labeled with c-Fos ($n = 6$/group). Brown punctate signals mean c-Fos activity. Scale bars, 200 μm.

(H) Quantification of c-Fos$^+$ cells per unit area in SolM, SolIM, and SolDL ($n = 6$/group; ordinary one-way ANOVA).

(I) Representative hippocampal sections from PTZ-treated mice labeled with c-Fos ($n = 6$/group). Scale bars, 500 μm. Insets show magnified images of CA3 and DG regions. Brown punctate signals mean c-Fos activity (scale bars, 50 μm).

(J) Quantification of c-Fos$^+$ cells per unit area in CA3 and DG ($n = 6$/group; ordinary one-way ANOVA). Data are presented as mean ± SEM. $^{**}p < 0.01$, $^{***}p < 0.001$, n.s., not significant ($p > 0.05$).

See also Figure S7.

Please cite this article in press as: Jia et al., Gut-brain cholinergic signaling mediates the antiseizure effects of *Bacteroides fragilis*, Neuron (2025), https://doi.org/10.1016/j.neuron.2025.11.029

whereas the hM3Dq group showed no significant difference (4.12 ± 0.27, $p = 0.47$) (Figures S7A and S7B). Consistently, c-Fos mapping revealed increased neuronal activity in the medial (SolM) and intermediate (SolIM) subregions of the NTS following either BF839 administration or activation of ChAT$^+$ cells, with a synergistic enhancement observed upon their combination—regions known to serve as key hubs for vagal input[60] (SolM: EGFP + BF839 + PTZ, 28.00 ± 1.46; hM3Dq + PTZ, 30.00 ± 1.69; hM3Dq + BF839 + PTZ, 41.17 ± 0.87; $p_{(EGFP + BF839 + PTZ)-(hM3Dq + BF839 + PTZ)} < 0.001$; $p_{(hM3Dq + PTZ)-(hM3Dq + BF839 + PTZ)} < 0.001$; SolIM: EGFP + BF839 + PTZ, 26.50 ± 1.31; hM3Dq + PTZ, 30.33 ± 1.72; hM3Dq + BF839 + PTZ, 39.67 ± 1.54; $p_{(EGFP + BF839 + PTZ)-(hM3Dq + BF839 + PTZ)} < 0.001$; $p_{(hM3Dq + PTZ)-(hM3Dq + BF839 + PTZ)} < 0.001$) (Figures 5G and 5H). In contrast, no significant changes were observed in the dorsolateral subregion (SolDL) (Figure 5H). Importantly, hippocampal activity in canonical seizure foci—CA3 (EGFP + BF839 + PTZ: 41.50 ± 1.18 or hM3Dq + PTZ: 43.17± 1.42 vs. hM3Dq + BF839 + PTZ: 25.70 ± 1.30; $p_{(EGFP + BF839 + PTZ)-(hM3Dq + BF839 + PTZ)} < 0.001$; $p_{(hM3Dq + PTZ)-(hM3Dq + BF839 + PTZ)} < 0.001$) and DG (EGFP + BF839 + PTZ: 35.83 ± 2.15 or hM3Dq + PTZ: 38.50 ± 2.28 vs. hM3Dq + BF839 + PTZ: 16.83 ± 1.82; $p_{(EGFP + BF839 + PTZ)-(hM3Dq + BF839 + PTZ)} < 0.001$; $p_{(hM3Dq + PTZ)-(hM3Dq + BF839 + PTZ)} < 0.001$)—was robustly suppressed by either intervention, with the strongest inhibition observed in the combined group (Figures 5I and 5J). Together, these results provide direct circuit-level evidence that colonic ChAT$^+$ cells mediate BF839-induced cholinergic signals via the vagus nerve to the NTS, thereby attenuating hippocampal hyperexcitability and reducing seizure activity. This establishes the colonic ChAT$^+$-vagus afferent pathway as a critical pathway for gut-brain signaling in BF839's role in seizure protection.

Next, we sought to conduct the functional verification on the vagal gut-brain axis mediated by ACh signals. Vagus nerve electroneurogram recording were used to assess whether colonic infusion of ACh or BF839 in anesthetized mice could elicit a vagal response (Figure S7C). To minimize potential confounding effects of isoflurane on vagal nerve activity, all recordings were conducted under a standardized anesthetic protocol using 1.75% isoflurane in 100% oxygen throughout the procedure.[61] The data indicated that both ACh (ACh: 5.09 ± 0.11 vs. saline: 4.02 ± 0.08; $p = 0.002$) and BF839 (BF839: 5.70 ± 0.20 vs. saline: 4.02 ± 0.08; $p < 0.001$) significantly elevated the total vagal firing rate compared with saline during the 120–180-s post-infusion window (Figures S7D and S7E). Notably, a decline in vagal firing was observed after infusion, albeit with distinct patterns: ACh led to a steeper reduction, while BF839 exhibited a more gradual decrease (Figure S7D). Statistical analysis further confirmed that significant differences in vagal firing persisted after the cessation of both ACh and BF839 infusions (i.e., after 180 s) relative to saline, with a marked distinction between the ACh and BF839 (ACh: 4.34 ± 0.10 vs. BF839: 5.40 ± 0.21; $p = 0.0089$) groups (Figure S7F). These results demonstrate that both ACh and BF839 can transmit signals to the central nervous system via the gut-vagus nerve axis, with BF839 showing a more sustained activation of the vagus nerve compared with ACh. We further examined the effects of intestinal perfusion of mecamylamine (MEC), a nicotinic AChR antagonist, on the vagal activity and the antiseizure effect of BF839. The results demonstrated a marked increase in vagal firing rate during the 120–180-s window following ACh infusion into the colon (Figure S7G). Subsequently, MEC was administered between 180 and 240 s, resulting in a significant reduction in the vagal firing rate (Figure S7G). Compared with the saline-treated ACh group, the MEC-treated ACh group exhibited a similar overall level of vagal firing (ACh + saline: 5.27 ± 0.11 vs. ACh + MEC: 4.77 ± 0.13; $p = 0.0744$), but specifically during the 180- to 240-s period, it showed a pronounced reduction in vagal firing compared with the ACh + saline group (ACh + saline: 6.70 ± 0.19 vs. ACh + MEC: 4.29 ± 0.08; $p < 0.001$) (Figures S7H and S7I). Importantly, administration of MEC alone, in the absence of ACh, did not significantly alter baseline neuronal firing rates, indicating that the observed suppression is specific to ACh-evoked activity (Figures S7H and S7I). These results provide compelling evidence that ACh transmits signals through nicotinic AChRs in the gut, relaying these signals to the brain via the vagus nerve. A similar experimental outcome was observed when MEC was administered following BF839 (Figure S7J). Specifically, compared with the BF839 group treated with saline, the BF839 + MEC group displayed a significant reduction in vagal firing rate (BF839 + saline: 5.51 ± 0.13 vs. BF839 + MEC: 4.55 ± 0.042; $p = 0.001$), particularly during the 180–240-s period post-MEC administration (BF839 + saline: 5.62 ± 0.12 vs. BF839 + MEC: 4.18 ± 0.033; $p < 0.001$) (Figures S7K and S7L). These observations reinforce the hypothesis that both ACh and BF839 modulate vagus nerve activity by activating nicotinic AChRs. Collectively, these results suggest that BF839 may elevate ACh expression in colonic tuft cells, leading to enhanced ChAT-mediated vagal signaling to the brain. This signaling likely contributes to the transmission of antiseizure neural signals, exerting an antiseizure effect through specific AChR activation.

To further validate whether the antiseizure effect of BF839 is dependent on the cholinergic signaling pathway, we conducted an investigation to examine the effect of MEC administration via intraperitoneal injection or oral gavage on the antiseizure efficacy of BF839 in mice. Mice were subjected to the same procedure as in the previous experiments. On the 22nd day of PTZ injection, the mice were administered an intragastric dose of 3 mg/kg of MEC 10 min after BF839 administration. Their behaviors were then recorded for 30 min for conducting an epileptic behavioral assessment. The findings of the experimental study indicated that, in comparison with mice that had been treated with BF839 alone, those that had been treated with MEC exhibited a pronounced deterioration of epileptic behaviors when induced with PTZ. Results demonstrated that MEC significantly increased the number of seizures in BF839-treated mice (BF839 + PTZ: 1.33 ± 0.21 vs. BF839 + MEC + PTZ: 2.50 ± 0.34; $p = 0.0071$) (Figure S7M). Seizure latency was also shortened in BF839-treated mice post-MEC compared with BF839 alone (BF839 + PTZ: 573.83 ± 23.44 s vs. BF839 + MEC + PTZ: 307.83 ± 23.21 s; $p < 0.001$) (Figure S7N). In contrast, seizure duration was prolonged in BF839 treated mice after MEC compared with BF839 alone (BF839 + PTZ: 434.33 ± 29.13 s vs. BF839 + MEC + PTZ: 695.67 ± 45.02 s; $p < 0.001$) (Figure S7O). MEC administration also exacerbated seizure severity in all BF839 groups (BF839 + PTZ: 1.42 ± 0.20 vs. BF839 + MEC + PTZ: 2.28 ± 0.13; $p = 0.0057$) (Figure S7P). These

Please cite this article in press as: Jia et al., Gut-brain cholinergic signaling mediates the antiseizure effects of *Bacteroides fragilis*, Neuron (2025), https://doi.org/10.1016/j.neuron.2025.11.029

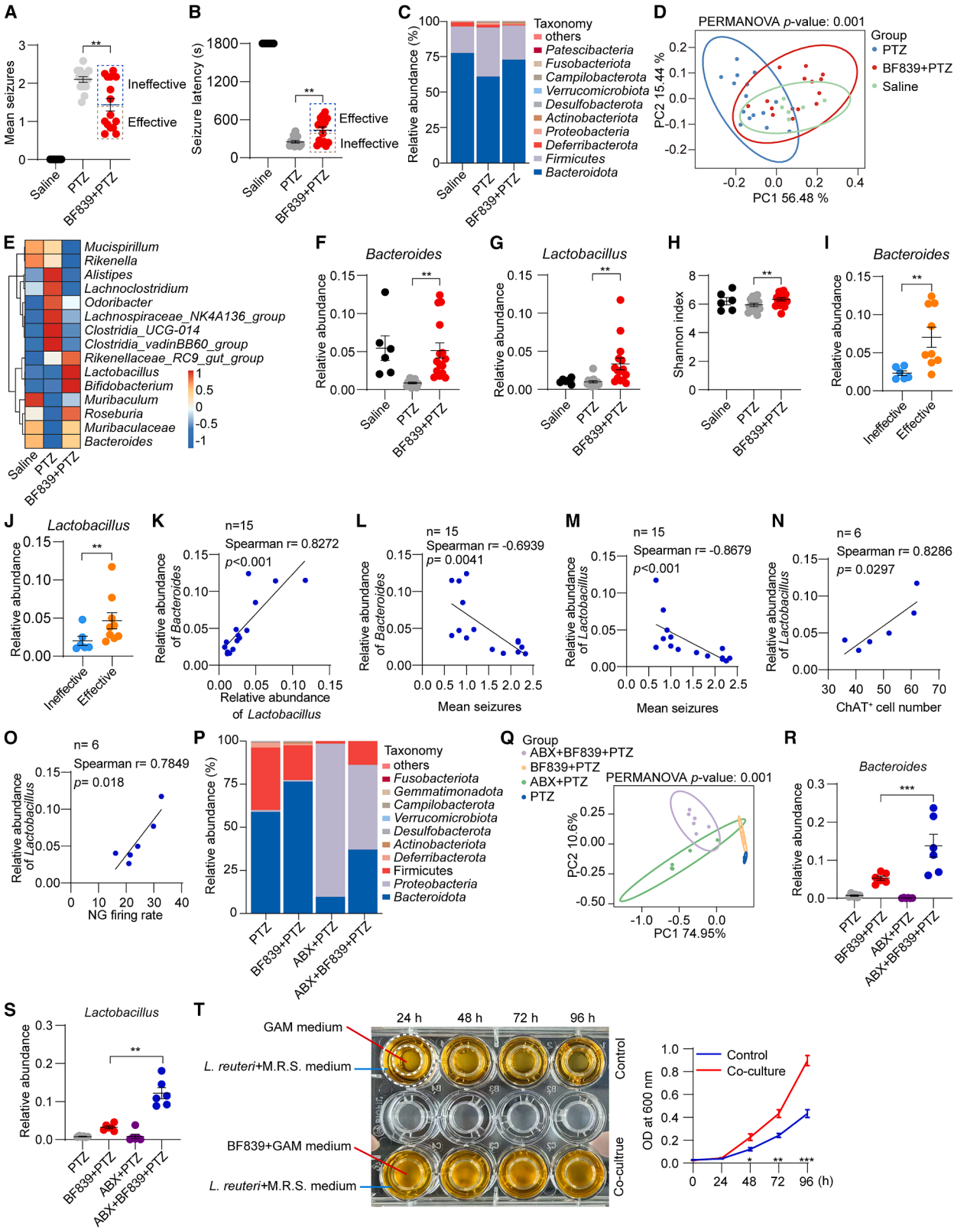

(legend on next page)

Please cite this article in press as: Jia et al., Gut-brain cholinergic signaling mediates the antiseizure effects of *Bacteroides fragilis*, Neuron (2025), https://doi.org/10.1016/j.neuron.2025.11.029

collective findings strongly suggest that the antiseizure effect of BF839 may be mediated by its modulation of the acetylcholinergic vagal signals from the gut to the brain via the NG and that MEC, by blocking these receptors, reversed the therapeutic efficacy of BF839.

The antiseizure effect of *B. fragilis* is associated with the intestinal colonization of *Lactobacillus*

As evidenced by the aforementioned results, BF839 treatment alleviated seizure activity in the PTZ-induced mouse model, mice in the BF839 group exhibited significantly fewer seizures (BF839 + PTZ: 1.44 ± 0.17 vs. PTZ: 2.10 ± 0.07; $p = 0.0011$), increased seizure latency (BF839 + PTZ: 463.07 ± 49.34 s vs. PTZ: 252.73 ± 19.69 s; $p = 0.0068$), and reduced seizure duration (BF839 + PTZ: 387 ± 48.62 s vs. PTZ: 565.67 ± 41.99 s; $p = 0.00996$) (Figures 6A, 6B, and S8A) after a 22-day interval. However, the antiseizure efficacy of BF839 exhibited notable inter-individual variability, leading to the classification of BF839-treated mice into effective and ineffective groups (Figures 6A, 6B, and S8A). Mice in the "BF839-effective" group exhibited a markedly lower seizure incidence (BF839-effective: 0.96 ± 0.09 vs. BF839-ineffective: 2.15 ± 0.07; $p < 0.001$) and seizure score (BF839-effective: 1.43 ± 0.07 vs. BF839-ineffective: 2.12 ± 0.06; $p < 0.001$) compared with those in the "BF839-ineffective" group (Figures S8B and S8C). To further examine potential factors contributing to individual variations in therapeutic efficacy of BF839 among PTZ-treated juvenile mice, we analyzed changes in gut microbiota composition using 16S rRNA sequencing of fecal samples from all experimental groups. In line with previous findings,[62] the gut microbiota of the experimental mice was dominated by the phyla *Bacteroidetes* and *Firmicutes* (Figure 6C). Principal coordinates analysis (PCoA) based on weighted UniFrac distances confirmed that PTZ treatment induced significant alterations in the bacterial community composition (Figure 6D). Notably, intragastric administration of BF839 led to a substantial increase in the relative abundance of *Bacteroides* (BF839 + PTZ: 0.05 ± 0.009 vs. PTZ: 0.009 ± 0.001; $p = 0.0024$) and *Lactobacillus* (BF839 + PTZ: 0.033 ± 0.008 vs. PTZ: 0.01 ± 0.001; $p < 0.001$) (Figures 6E–6G). Measures of alpha diversity indicated that BF839 increased gut microbiota diversity (BF839 + PTZ: 6.33 ± 0.11 vs. PTZ: 5.94 ± 0.11; $p = 0.0253$) (Figure 6H). Further validation using de Man, Rogosa, and Sharpe (MRS) agar cultivation at 37°C demonstrated that fecal samples from BF839-treated mice contained significantly higher counts of *Lactobacillus* compared with the PTZ group after 22 days of treatment (BF839 + PTZ: 67,333.33 ± 8,871.93 CFU/g vs. PTZ: 17,500 ± 3,211.96 CFU/g; $p = 0.008$) (Figures S8D and S8E). These results align with the sequencing data on gut microbiota composition. A comparative analysis of the microbiota composition between the effective and ineffective groups revealed significant differences in gut microbiota structure between them (Figures S8F and S8G). However, no significant differences were observed in the alpha diversity of the gut microbiota between the two groups (BF839 + PTZ: 6.05 ± 0.14 vs. PTZ: 5.85 ± 0.27; $p = 0.4559$) (Figure S8H). The relative abundance of *Bacteroides* and *Lactobacillus* in the feces of mice in the BF839-effective group showed elevated levels in comparison with the BF839-ineffective group (*Bacteroides*, BF839-ineffective: 0.02 ± 0.003 vs. BF839-effective: 0.07 ± 0.01; $p = 0.028$) (*Lactobacillus*, BF839-ineffective: 0.047 ± 0.011 vs. BF839-effective: 0.02 ± 0.0059; $p = 0.026$) (Figures 6I and 6J). Interestingly, the Spearman correlation analysis revealed a positive correlation between the relative abundance of *Bacteroides* and *Lactobacillus* (Figure 6K). In contrast, a negative correlation was identified between the relative abundances of *Bacteroides* and

Figure 6. Subgroup differences in the antiseizure effects of BF839 are associated with *Lactobacillus* abundance

(A) Average total number of seizures per animal per day with 12 PTZ injections (saline, $n = 6$; PTZ and BF839, $n = 15$) (unpaired *t* test).
(B) Seizure latency following the final PTZ injection (saline, $n = 6$; PTZ and BF839, $n = 15$) (Mann-Whitney test).
(C) Microbiota composition at the phylum level in saline ($n = 6$), PTZ ($n = 15$), and BF839 + PTZ ($n = 15$) treatment groups.
(D) PCoA of gut microbiota composition at the genus level, based on the weighted UniFrac matrix for each group on day 22 after PTZ induction, as described in Figure 2A (saline, $n = 6$; PTZ and BF839, $n = 15$).
(E) Hierarchical clustering of the relative abundances of the top 15 bacterial genera across treatment groups (BF839 + PTZ, BF839, and saline). Color gradient reflects the relative abundance of each taxon normalized to its minimum value across treatment groups (BF839 + PTZ, BF839, and saline). Blue indicates lower abundance, and red indicates higher abundance relative to this baseline.
(F) Relative abundance of *Bacteroides* (saline, $n = 6$; PTZ and BF839, $n = 15$) (Mann-Whitney test).
(G) Relative abundance of *Lactobacillus* (saline, $n = 6$; PTZ and BF839, $n = 15$) (Mann-Whitney test).
(H) Shanon α-diversity index of grouped data (saline, $n = 6$; PTZ and BF839, $n = 15$) (unpaired *t* test).
(I) Differences in *Bacteroides* abundance between individuals showing effective and ineffective responses to BF839 treatment (ineffective, $n = 6$; effective, $n = 9$) (Mann-Whitney test).
(J) Differences in *Lactobacillus* abundance between individuals showing effective and ineffective responses to BF839 treatment (ineffective, $n = 6$; effective, $n = 9$) (Mann-Whitney test).
(K) Positive correlation between the relative abundances of *Bacteroides* and *Lactobacillus*.
(L) Negative correlation between *Bacteroides* abundance and mean seizure frequency.
(M) Negative correlation between *Lactobacillus* abundance and mean seizure frequency.
(N) Positive correlation between *Lactobacillus* abundance and the number of $ChAT^+$ cells in the colon.
(O) Positive correlation between *Lactobacillus* abundance and vagus nerve firing rate.
(P) Microbiota composition at the phylum level in each group ($n = 6$/group), as described in Figure 2M.
(Q) PCoA of gut microbiota composition at the genus level, based on the weighted UniFrac matrix for each group on day 22 after PTZ induction ($n = 6$/group).
(R) Relative abundance of *Bacteroides* (left) and *Lactobacillus* (right) in each group ($n = 6$/group) (ordinary one-way ANOVA).
(S) Representative image of BF839 co-cultured with *Lactobacillus reuteri* ($n = 6$/group).
(T) OD values measured at different time points ($n = 3$/group) (Mann-Whitney test).
See also Figures S8–S11 and Table S4.

Please cite this article in press as: Jia et al., Gut-brain cholinergic signaling mediates the antiseizure effects of *Bacteroides fragilis*, Neuron (2025), https://doi.org/10.1016/j.neuron.2025.11.029

Lactobacillus and the mean number of seizures (Figures 6L and 6M). This suggests that the ecological niche of *Lactobacillus* within the host's gut may be a determining factor in the antiseizure efficacy of BF839. It is noteworthy that a positive correlation was observed between the relative abundance of *Lactobacillus* and the $ChAT^+$ cells in the colon (Figure 6N). A positive correlation was also identified between the relative abundance of *Lactobacillus* and the recorded firing rate of the vagal ganglia in mice (Figure 6O), highlighting the potential interplay between these microbial taxa in mediating the antiseizure effects of BF839 via activation of gut-brain cholinergic signaling.

These findings underscore the association between intragastric BF839 administration and reduced seizures in PTZ-induced epileptic mice and suggest that these effects are correlated with the colonization of *Lactobacillus*, which may contribute to the maintenance of host gut microbial homeostasis. We next sought to investigate whether augmenting the ecological niche of *Bacteroides* in the gut by the administration of the ABX prior to the BF839 treatment also facilitates the colonization of *Lactobacillus*, which may participate in the antiseizure effect of BF839, by examining the gut microbiota composition of mice from different groups after treatment with ABX and BF839. The administration of ABX resulted in alterations to the gut microbiota composition at the phylum level, when compared with mice that had not undergone ABX treatment (Figures 6P and 6Q). In particular, the administration of BF839 after ABX treatment resulted in a significant increase in the abundance of not only *Bacteroides* (ABX + BF839 + PTZ: 0.14 ± 0.03 vs. BF839 + PTZ: 0.053 ± 0.005; $p < 0.001$) but also *Lactobacillus* (ABX + BF839 + PTZ: 0.12 ± 0.014 vs. BF839 + PTZ: 0.033 ± 0.004; $p = 0.0043$) in mice compared with those treated with BF839 alone (Figures 6R and 6S). The physical integrity of the intestinal barrier, constituted by epithelial cells, is of pivotal importance in maintaining the homeostasis of the gut microbiota, and vice versa. Subsequently, we analyzed the effect of BF839 on the integrity of the intestinal barrier using immunostaining of tight junction proteins, including Zonula occludens-1 (ZO-1) and occludin, in colon tissues of mice. Mice treated with PTZ exhibited a notable reduction in the number of ZO-1-positive cells and the relative fluorescence intensity of ZO-1, in comparison with the saline group (ZO-1 cell number, PTZ: 22.50 ± 2.32 vs. BF839 + PTZ: 69.83 ± 3.09; $p = 0.0146$) (intensity, PTZ: 0.52 ± 0.061 vs. BF839 + PTZ: 0.88 ± 0.041; $p = 0.002$) (Figure S9A). In addition, BF839 administration resulted in a significant increase in the area of occludin-positive cells (PTZ: 1.62 ± 0.16 vs. BF839 + PTZ: 3.83 ± 0.34; $p < 0.001$) and the relative fluorescence intensity of occludin (PTZ: 0.55 ± 0.043 vs. BF839 + PTZ: 0.94 ± 0.082; $p = 0.0409$) compared with mice in the PTZ alone group (Figure S9A). We also evaluated the integrity of the intestinal barrier by performing the immunostaining of ZO-1 and occludin in the presence of BF839 and ABX treatments. The ABX pretreatment resulted in a notable elevation in the expression of ZO-1 (ABX + BF839 + PTZ: 70.00 ± 2.02 vs. PTZ: 17.00 ± 1.62; $p < 0.001$) and occludin (ABX + BF839 + PTZ: 3.68 ± 0.23 vs. PTZ: 1.78 ± 0.14; $p < 0.001$) in the colon when compared with the PTZ group (Figure S9B), thereby indicating that BF839 plays a role in safeguarding the integrity of the intestinal barrier and maintaining the homeostasis of the gut microbiota. Taken together, these results suggest that BF839 confers protection by ameliorating PTZ-induced dysbiosis and damage to the intestinal mucosal barrier.

To further elucidate the mechanism by which *B. fragilis* promotes *Lactobacillus* growth, we performed anaerobic co-culture experiments using a *Lactobacillus reuteri* (*L. reuteri*) strain isolated from BF839-treated mouse feces on MRS selective medium and identified through 16S rRNA sequencing (Table S4), allowing direct assessment of their commensal interaction (Figure 6T). The results, as indicated by optical density (OD) values, indicated an increase in *L. reuteri* abundance when co-cultured with BF839, suggesting that BF839 metabolic byproducts may stimulate *L. reuteri* growth (Figure 6T). To validate this promotion of *Lactobacillus* colonization by *B. fragilis in vivo*, we administered BF839, *L. reuteri*, or the mixture of BF839 and *L. reuteri* to mice by gavage for 5 consecutive days (Figure S10A). The feces were collected and homogenized, followed by centrifugation to obtain the supernatant for subsequent dilution and plating. The results revealed that, compared with the administration of *L. reuteri* alone, the mixture of BF839 and *L. reuteri* by gavage significantly increased the levels of *L. reuteri* in the feces of the mice (*L. reuteri*: 30,000 ± 2,966.47 CFU/g vs. *L. reuteri* + BF839: 59,833.33 ± 3,978.41 CFU/g; $p = 0.0011$; Figure S10B). To confirm the facilitating effect of BF839 on *L. reuteri*, we employed a mixture of BF839 and *L. reuteri* or a mixture of *Escherichia coli* (*E. coli*) and *L. reuteri* and inoculated them in a fastidious anaerobic nutrient plate supplemented with 0.5% yeast extract to evaluate their growth status. Daily observation of colony growth over 7 days revealed a co-cultivation phenomenon between *L. reuteri* and BF839, with colonies forming adjacent to each other, whereas no such phenomenon occurred with *L. reuteri* and *E. coli* (Figures S10C and S10D).

To investigate the mechanisms by which *Bacteroides* promotes the growth and intestinal colonization of *Lactobacillus*, we used microbial community metabolic modeling (MICOM), a constraint-based microbial community modeling approach, to reconstruct gut microbial models from PTZ- or BF839 + PTZ-treated mice.[63] Simulations revealed that BF839 intervention markedly increased the relative flux of metabolites supplied to *Lactobacillus* compared with the PTZ-only group (Figure S10E). These findings suggest that the *Bacteroides*-enriched microbial communities in BF839-treated mice generate a metabolic environment conducive to *Lactobacillus* growth and colonization. KEGG pathway analysis of *Bacteroides*-derived metabolites revealed several metabolites with elevated relative levels in BF839-treated communities that are important for *Lactobacillus* proliferation. Notably, *Bacteroides* contributed increased relative abundances of L-cysteine and glycine—amino acids essential for the growth of many *Lactobacillus* species (Figure S11A).[64,65] Additionally, metabolites including L-malate, L-aspartate, hydrogen phosphate, acetate, and L-lactate were predicted to support *Lactobacillus* energy metabolism by feeding into pyruvate and acetyl-coenzyme A (CoA) biosynthesis pathways (Figures S11A and S11B).[66] These metabolites play central roles in glycolysis and amino acid metabolism, ultimately promoting bacterial proliferation and colonization (Figure S11B). Collectively, these results indicate that BF839-induced modulation of the gut microbiota

Please cite this article in press as: Jia et al., Gut-brain cholinergic signaling mediates the antiseizure effects of *Bacteroides fragilis*, Neuron (2025), https://doi.org/10.1016/j.neuron.2025.11.029

CellPress

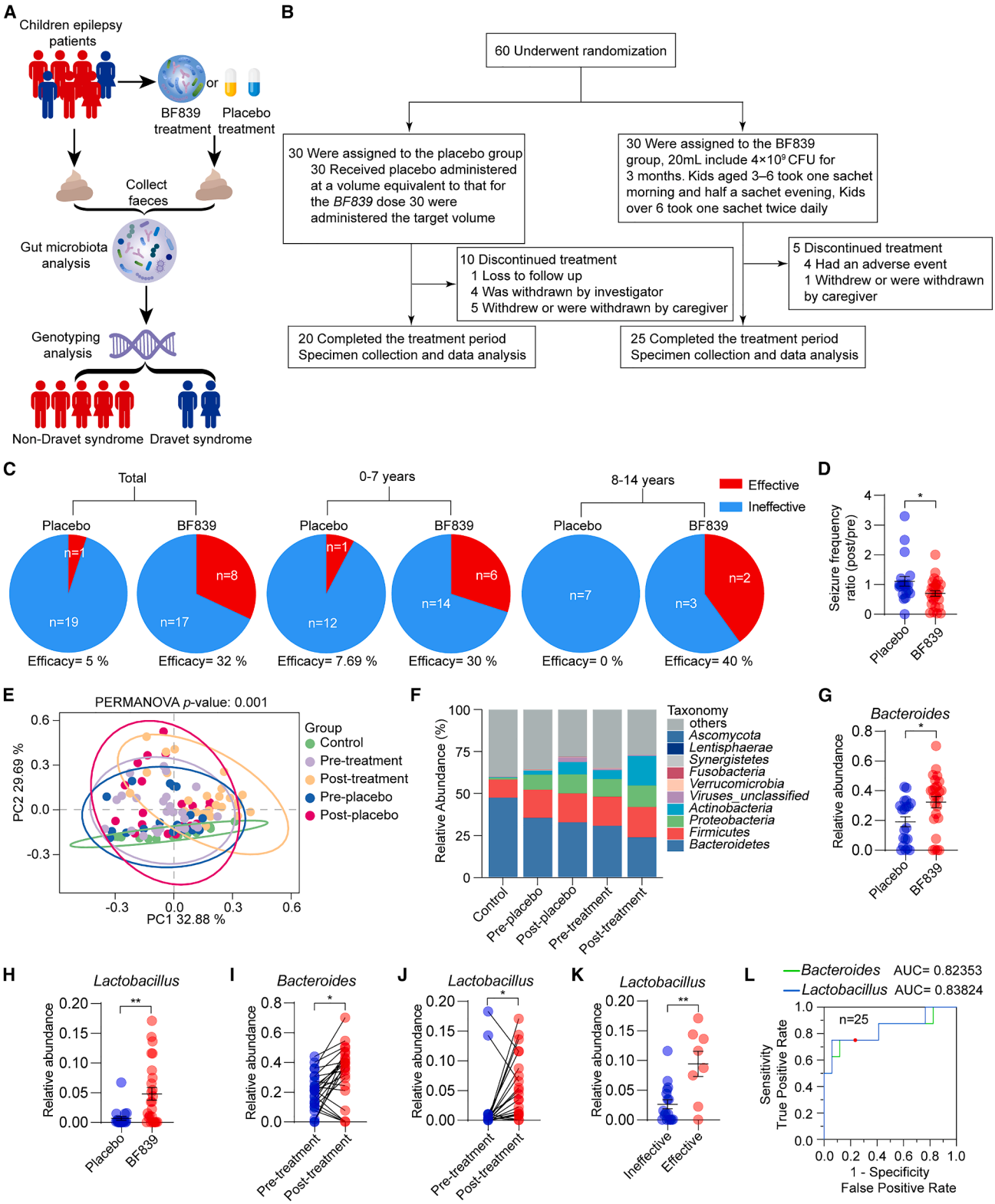

Figure 7. Participants and therapeutic outcomes of the oral BF839 pilot study in children with epilepsy

(A) Flowchart illustrating the clinical trial design used in this study.

(B) Enrollment details and results of the clinical trial.

(legend continued on next page)

Please cite this article in press as: Jia et al., Gut-brain cholinergic signaling mediates the antiseizure effects of *Bacteroides fragilis*, Neuron (2025), https://doi.org/10.1016/j.neuron.2025.11.029

enhances the availability of metabolites supporting *Lactobacillus* growth, thereby facilitating its expansion in the colon. This metabolic shift may contribute to the antiseizure effects observed following BF839 treatment. Collectively, these findings highlight that enhancing the ecological niche of *Bacteroides* and *Lactobacillus* in the gut significantly augments the antiseizure efficacy of BF839.

Therapeutic efficacy of *B. fragilis* in children with refractory epilepsy

Based on animal studies showing that treatment with BF839 can increase the abundance of *Lactobacillus* in the colon, we conducted a validation study in humans to investigate whether BF839 has a comparable ability to increase the abundance of *Lactobacillus* in the intestinal tract of children with refractory epilepsy. To evaluate the translational potential of the antiseizure effects of *B. fragilis* observed in the PTZ-induced mouse model, we included 60 patients with refractory epilepsy from the outpatient department of Shenzhen Children's Hospital between February 2021 and January 2022. All participants were local residents of Shenzhen with similar dietary habits, voluntarily consented to participate, and met the inclusion criteria (Table S5). Participants were randomized to receive either placebo or BF839 for 3 months while maintaining their regular diet and anticonvulsant medication (Figures 7A and 7B). Baseline characteristics, including demographics, seizure types, and antiseizure medication use, were well balanced between the placebo and treatment groups (Tables S5 and S6). Specifically, the distribution of sex was similar in the BF839 group (68.97% male, 31.03% female) and the placebo group (50% male, 50% female), with no significant difference observed ($p = 0.359$). Post-treatment clinical characteristics are provided in Table S7. Significantly higher efficacy was observed in the BF839 group, with 32% of patients showing effective seizure reduction compared with 5% in the placebo group ($p = 0.0224$) (Figure 7C). Notably, the efficacy of BF839 remained consistent across different age groups (0–7 and 8–14 years) ($p = 0.0973$, 0.1618) (Figure 7C). To quantify treatment effects, we calculated the normalized seizure frequency ratio (post-treatment/pre-treatment). BF839-treated patients exhibited a significantly lower ratio (0.70 ± 0.09) compared with the placebo group (1.10 ± 0.16, $p = 0.0117$) (Figure 7D), indicating a reduction in seizure frequency following treatment.

Adverse events were monitored throughout the trial, with mild events including abdominal pain (1/30), diarrhea (1/30), constipation (1/30), and language regression (1/30) observed in approximately 13.3% of the treatment group. These side effects were transient, resolving within 1 week, and no significant adverse events were reported in the placebo group (Table S8). Analysis of 16S rRNA sequencing of fecal samples showed no significant differences in gut microbiota diversity between the groups after treatment (Figure S12A). However, compositional changes at the genus (Figure 7E) and phylum (Figure 7F) levels were observed following BF839 treatment, with an increase in the relative abundance of *Bacteroides* (BF839: 0.31 ± 0.039 vs. placebo: 0.19 ± 0.033; $p = 0.0262$) and *Lactobacillus* (BF839: 0.048 ± 0.011 vs. placebo: 0.007 ± 0.003; $p = 0.0015$) compared with the placebo group (Figures 7G and 7H). Further analysis showed significant changes in the relative abundance of *Bacteroides* and *Lactobacillus* after treatment, with levels of *Bacteroides* rising from 0.19 ± 0.025 to 0.31 ± 0. 0397 ($p = 0.013$) and *Lactobacillus* increasing from 0.015 ± 0.009 to 0.04 ± 0.01 ($p = 0.0194$) (Figures 7I and 7J). Notably, patients with good treatment efficacy exhibited significantly higher levels of *Lactobacillus* compared with those with poor efficacy (ineffective: 0.026 ± 0.008 vs. effective: 0.096 ± 0.02; $p < 0.001$) (Figure 7K). Stratified analysis revealed that the treatment was more effective in patients with non-Dravet syndrome (36.84%) compared with those with Dravet syndrome (20%) ($p = 0.2733$) (Figure S12B). PCoA indicated no significant differences in beta diversity between the two groups (Figure S12C). In patients with non-Dravet syndrome, BF839 treatment effectively increased the relative abundance of *Bacteroides* (from 0.21 ± 0.03 to 0.38 ± 0.04; $p = 0.0014$) and *Lactobacillus* (from 0.018 ± 0.012 to 0.054 ± 0.011; $p = 0.0346$), while no significant changes were observed in the Dravet group (*Bacteroides* from 0.13 ± 0.041 to 0.1 ± 0.05; $p = 0.728$) (*Lactobacillus* from 0.003 ± 0.002 to 0.031 ± 0.028; $p = 0.3412$) (Figures S12D and S12E). Alpha diversity remained unchanged in both groups (Figure S12F).

To evaluate the predictive value of gut microbiota composition for treatment response, we generated receiver operating characteristic (ROC) curves based on the relative abundances of *Bacteroides* and *Lactobacillus* (Figure 7L). These models demonstrated robust discrimination of favorable outcomes in pediatric patients with refractory epilepsy, yielding area under the curve (AUC) values of 0.8235 and 0.8382, respectively, indicative of strong predictive performance. BF839 treatment markedly modulated gut microbiota composition, notably increasing the relative abundance of these beneficial taxa

(C) Overall therapeutic efficacy of BF839, including age-specific subgroup analysis.
(D) Normalized seizure frequency ratio (post-treatment/pre-treatment) was used to quantify therapeutic response (unpaired *t* test).
(E) PCoA plot showing gut microbiota composition at the genus level based on the weighted UniFrac matrix for each group (control, $n = 30$; placebo, $n = 20$; BF839, $n = 25$).
(F) Relative abundance of gut bacterial phyla before and after the probiotic treatment in the control ($n = 30$), placebo ($n = 20$), and BF839 ($n = 25$) groups.
(G) Relative abundance of *Bacteroides* (placebo, $n = 20$; BF839, $n = 25$) (Mann-Whitney test).
(H) Relative abundance of *Lactobacillus* (placebo, $n = 20$; BF839, $n = 25$) (unpaired *t* test).
(I) Relative abundances of *Bacteroides* before and after BF839 treatment ($n = 25$/group) (unpaired *t* test).
(J) Relative abundances of *Lactobacillus* before and after BF839 treatment ($n = 25$/group) (unpaired *t* test).
(K) Comparison of *Lactobacillus* abundance between participants with ineffective and effective responses to BF839 treatment (ineffective, $n = 17$; effective, $n = 8$) (unpaired *t* test).
(L) ROC curve analysis assessing BF839 treatment efficacy in relation to patient gender and age. Data are presented as mean ± SEM.
See also Figure S12 and Tables S5, S6, S7, and S8.

Please cite this article in press as: Jia et al., Gut-brain cholinergic signaling mediates the antiseizure effects of *Bacteroides fragilis*, Neuron (2025), https://doi.org/10.1016/j.neuron.2025.11.029

(Figures 7F–7H). Clinical response to BF839 exhibited inter-individual variability that correlated with host genetic backgrounds linked to epilepsy. Importantly, the antiseizure efficacy of BF839 was positively associated with successful gut colonization by *Bacteroides* and *Lactobacillus* (Figure 7K), and this relationship was preserved across genetically diverse individuals, underscoring the microbiota's role in mediating individualized therapeutic responses to probiotic intervention. To further investigate the potential mechanistic interplay between BF839 and *Lactobacillus* in mediating therapeutic efficacy, we performed microbial community metabolic modeling using MICOM. This analysis revealed a specific enrichment of succinate—but not acetate or nicotinate—in therapy responders, consistently observed across both mouse models and human patients (Figures S12G and S12H). Previous work has shown that succinate, as the natural ligand for succinate receptor 1 (SUCNR1), activates this receptor on intestinal epithelial ChAT$^+$ cells and may thereby induces ACh release along the gut-brain axis.[54] Taken together, these findings support the interpretation that the therapeutic efficacy of BF839 may depend, at least in part, on a cooperative microbial mechanism involving *Lactobacillus*, which potentiates cholinergic signaling to alleviate seizures. In summary, findings from our clinical trial are consistent with those from preclinical studies, reinforcing the therapeutic potential of BF839 in managing refractory epilepsy in children.

DISCUSSION

This study identifies a previously unrecognized gut-brain cholinergic signaling axis as a central mediator of the antiseizure effects of *B. fragilis*, thereby extending current concepts of gut microbiota-brain communication in epilepsy. Whereas most prior research has emphasized the role of circulating microbial metabolites (e.g., short-chain fatty acids and tryptophan derivatives) in modulating neuronal excitability, our findings demonstrate that ACh, released by colonic ChAT$^+$ tuft cells and transmitted via the vagus nerve to the brain, serves as a direct neural conduit for microbial influence on seizures. This represents a paradigm shift in understanding how gut microbes regulate brain activity, moving beyond metabolic signaling to uncover a structurally and functionally defined neural circuit.

Choline, an essential nutrient and neurotransmitter, plays a critical role in neuroprotection and neurodevelopment.[22,67,68] Whereas previous chemogenetic studies have largely focused on central cholinergic circuits in epilepsy management,[20] our study identifies a previously unrecognized peripheral pathway in which BF839 upregulates ChAT expression in colonic cells, enhances ACh signaling to NG neurons, and ultimately suppresses hippocampal hyperexcitability. Consistent with recent reports, colonic ChAT$^+$ epithelial cells are largely tuft cells, which can sense microbial-derived cues via transient receptor potential cation channel subfamily M member 5-dependent chemosensory pathways and, through the interleukin (IL)-25-group 2 innate lymphoid cell (ILC2)-IL-13 axis, engage immune feedback that amplifies their expansion and cholinergic output.[47,54,69–72] BF839 may act along this integrated chemosensory-immune circuit, although the precise upstream mediators remain to be defined. The co-localization of ChAT$^+$ cells with synapsin-1 in the colonic cells, along with the retrograde neural tracing between the ChAT$^+$ colonic cells and the NG, suggests neural characteristics and an ability to transmit neural signals from the gut to the brain. Chemogenetic manipulations demonstrated that the integrity of the colonic ChAT$^+$-NG circuit is indispensable for BF839's therapeutic efficacy: targeted ablation of colonic ChAT$^+$ cells, vagotomy, or nicotinic receptor blockade abolished its antiseizure effects, whereas chemogenetic activation of these neurons potentiated BF839-mediated seizure suppression. Collectively, these data indicate that this ascending cholinergic pathway is not sufficient by itself but is necessary and acts in a permissive, modulatory manner to amplify BF839-mediated seizure suppression. These findings provide circuit-level evidence for a microbiota-dependent cholinergic pathway that regulates epileptogenesis. Importantly, BF839 selectively elevated choline levels in the gut and brain, but not in systemic circulation, underscoring the localized and neuronally restricted nature of this signaling route. Previous research has predominantly explored how gut microbiota and its metabolites influence the central nervous system via the bloodstream.[73,74] However, neural pathways, particularly the vagus nerve, also play a pivotal role in transmitting signals from the gut microbiota to the brain, including the perception of gastrointestinal information.[75,76] Emerging evidence underscores the critical role of vagal cholinergic signals in regulating various physiological functions.[44,55,77] While cholinergic signaling and ChAT$^+$ cells are also abundant in the proximal small intestine,[78,79] both the microbial niche[49,50] and our experimental data (Figures 4M, 6M, and 6N; Video S1) indicate that BF839 predominantly engages colonic ChAT$^+$ cells to mediate gut-brain communication and seizure protection. Future studies will be of interest to determine whether proximal intestinal cholinergic pathways may also participate in mediating microbiota-based modulation of seizure susceptibility under specific microbial or pathophysiological conditions. This study presents a novel probiotic mechanism in seizure, proposing that intestinal ChAT signaling is transmitted to the brain primarily through the vagus nerve rather than via the bloodstream.[80–82]

Our findings point to a multi-timescale mechanism by which BF839 exerts its antiseizure effects through gut-brain communication. The acute effects are evidenced by the rapid increase in vagal nerve activity within minutes of intestinal perfusion with BF839, suggesting that microbial metabolites can rapidly activate vagal afferents, consistent with recent findings.[49] In contrast, the chronic antiseizure effects coincide with the establishment of intestinal colonization and the remodeling of the gut microbiota. These longer-term effects are likely driven by sustained vagal input to central nuclei such as the NTS, leading to downstream modulation of limbic structures implicated in seizure regulation. Our current results suggest that BF839 may act through a two-phase model: rapid vagal activation via microbial metabolites and longer-term neuroplastic adaptations sustained by sustained cholinergic signaling. Recognizing and dissecting these distinct timescales will be critical for optimizing probiotic-based therapies for epilepsy and other neurodevelopmental conditions. Our findings reveal that the vagus nerve contributes not only to the acute but also to the sustained antiseizure effects of *B. fragilis*,

Please cite this article in press as: Jia et al., Gut-brain cholinergic signaling mediates the antiseizure effects of *Bacteroides fragilis*, Neuron (2025), https://doi.org/10.1016/j.neuron.2025.11.029

highlighting a chronic neuromodulatory role of gut-brain signaling. This extends current understanding of gut-brain cholinergic signaling by revealing its role in regulating brain excitability across both acute and chronic timescales, with implications for clinical translation. Additionally, these findings demonstrate that while acute VNS alone exerted limited seizure-suppressive effects, the combined VNS and BF839 treatment yields enhanced antiseizure efficacy, highlighting the potential of a personalized, probiotic-based therapy tailored to individual variations in vagus nerve activity and the intestinal colonization capacity of specific bacterial strains, which could be particularly beneficial for managing seizures in refractory epilepsy.

A positive correlation has been identified between a *Bacteroides*-dominated gut microbiome in late infancy and subsequent neurodevelopment.[83] However, substantial gaps remain in our understanding of individual variability in microbiome-based interventions and the underlying molecular mechanisms relevant to human clinical conditions. Building on prior evidence that gastrointestinal dysfunction and gut dysbiosis contribute to seizure susceptibility[29,84] and that specific bacteria enriched by the KD mediate antiseizure benefits,[14] our study reveals an ecological dimension of BF839 action: its antiseizure efficacy was strongly associated with the intestinal colonization of *Lactobacillus*. By promoting *L. reuteri* growth, BF839 appears to stabilize microbial community dynamics while simultaneously enhancing cholinergic gut-brain signaling. This cooperative interaction suggests that BF839 may function as a keystone strain, orchestrating both host-microbe and microbe-microbe networks toward neuroprotection.[9,85] The association between *Lactobacillus* abundance and seizure suppression was consistently observed across both mouse models and pediatric patients, supporting a precision-microbiome therapeutic framework in which baseline microbial ecology shapes probiotic responsiveness. Moreover, our findings indicate that the therapeutic benefit of BF839 may depend, at least in part, on a cooperative interaction with *Lactobacillus*, whereby microbial succinate production—previously reported to activate SUCNR1 on intestinal ChAT$^+$ cells—enhances cholinergic signaling along the gut-brain axis, thereby contributing to seizure suppression.[54]

Clinically, our pediatric trial not only validates the translational efficacy of BF839 but also highlights the necessity of personalized probiotic strategies that integrate host genetics, microbial ecology, and epilepsy subtype. Consistent with our preclinical findings, trial participants could be stratified into responders and non-responders, with therapeutic efficacy positively correlated with gut *Lactobacillus* abundance. Further investigations are warranted to optimize the *Bacteroides-Lactobacillus* compositional ratio and to elucidate its conserved mechanistic role in seizure protection across both mouse and human models. Host genetic background further shapes the capacity to harbor and interact with specific microbial communities, as demonstrated by the association between the lactase gene and the *Bifidobacterium* genus.[86] The attenuated response observed in Dravet syndrome underscores the critical importance of tailoring microbiome-based interventions to distinct disease contexts.

Taken together, this study provides a comprehensive framework linking microbial ecology, gut-brain cholinergic circuitry, and clinical efficacy in epilepsy. By uncovering a neural mechanism of microbial action, we extend the scope of microbiota-brain research beyond metabolic communication and propose *B. fragilis* as a prototype for circuit-targeted, precision microbiome therapies. More broadly, these results highlight that the vagal sensory pathway mediates both acute microbial signaling and sustained neuromodulatory control over brain excitability, with particular therapeutic relevance in early life—a critical window for intervention in pediatric epilepsy when gut microbiota and vagal circuitry are highly plastic. Although the microbiota-vagus-brain axis represents an evolutionarily conserved pathway with relevance across the lifespan, our study addresses a critical unmet need in pediatric refractory epilepsy, advancing mechanistic understanding and opening new avenues for microbiota-based precision interventions in childhood epilepsy.

Limitations of the study

This study provides mechanistic and translational insights into the antiseizure effects of BF839, revealing a critical role for cholinergic signaling within the gut-vagus-brain axis and its impact on hippocampal excitability. Nevertheless, several limitations should be acknowledged. First, the complex, bidirectional interactions between the gut microbiota and central neural networks in epileptogenesis remain incompletely understood. Even well-characterized biomarkers, such as dendritic spine density, exhibit stage- and cell-type-specific variability, limiting their reliability as consistent indicators of probiotic-mediated antiseizure effects.

Second, the clinical trial duration of 3 months limits the assessment of long-term outcomes, including seizure frequency, cognitive trajectories, and quality of life. Moreover, our cohort consisted primarily of children with drug-resistant epilepsy who were already receiving conventional antiseizure medications, leaving the efficacy of BF839 in newly diagnosed patients or treatment-naive children untested.

Third, environmental and lifestyle factors—including diet, micronutrient intake, and other exposures—can influence gut microbiota composition, and although baseline characteristics were rigorously controlled, residual confounding cannot be excluded. The sample size (n = 30 per group), determined based on prior estimations to ensure adequate statistical power for the primary endpoints, may nonetheless be underpowered to detect more subtle treatment effects influenced by clinical heterogeneity.

Finally, while our preclinical data demonstrate robust modulation of cholinergic gut-brain signaling and seizure suppression, translation to broader pediatric populations requires caution. Multi-center trials with harmonized protocols, longer follow-up, and comprehensive metadata collection—including dietary, genetic, and microbiome profiles—are warranted to validate the generalizability and durability of BF839-mediated antiseizure effects.

RESOURCE AVAILABILITY

Lead contact

Requests for further information, resources, and reagents should be directed to and will be fulfilled by the lead contact, Xin-an Liu (xa.liu@siat.ac.cn).

Materials availability

This study did not generate new, unique reagents.

Data and code availability

- All data supporting the findings of this study are available from the lead contact upon reasonable request. Y.J. and X.-a.L. had full and unrestricted access to all animal and human data generated in this study.
- This paper does not report original code.
- Any additional information required to reanalyze the data reported in this paper is available from the lead contact upon request.

ACKNOWLEDGMENTS

This work was supported by financial support from the Shenzhen Science and Technology Program (KCXFZ20211020163549011 and JCYJ20250604183013017 to X.-a.L., JCYJ20210324135211030 to D.C., and JCYJ20250604182920028 to Z.C.), the National Natural Science Foundation of China (NSFC) (32371213 to X.-a.L., 32000710 to Z.C., and U20A2016 to Z.C.), Shenzhen Medical Research Funds (D2301002 to X.-a.L.), the Guangdong Basic and Applied Basic Research Foundation (2023A1515011743 to X.-a.L., 2022A1515110624 to Y.J., and 2019A1515110190 to Z.C.), the Hubei Provincial Science and Technology Program (JCZRQN202500935 to Y.J.), the STI2030-Major Projects (2022ZD0207100 to Z.C.), the Shenzhen Key Basic Research Project (JCYJ20200109115641762 to Z.C.), the Technology and Innovation Commission of Shenzhen (ZDSYS20190902093601675 to Z.C.), the Sanming Project of Medicine in Shenzhen (SZSM202311028 to D.C.), the Epilepsy Research Foundation of Chinese Association Against Epilepsy (CU-C-2021-02 to D.C.), and Shenzhen Clinical Research Center (20220819113341005 to D.C.).

AUTHOR CONTRIBUTIONS

X.-a.L., Z.C., and D.C. designed this study. H.C., D.C., J.M., J.D., J. Liao, Y.J., and X.-a.L. recruited and supervised the participants and performed all clinical procedures. Y.J., Y.C., Q.Z., L.L., and H.C. collected and analyzed the clinical data. Y.J., Q.Z., S.C., H.C., J. Li, F.H., S.J., X.J., J.R., and F.M. completed the animal experiment. Y.J., H.C., and J. Li completed EEG recording and data analysis. Y.J., J. Li, S.J., and X.J. performed the preparation, processing, and sequencing of fecal samples. Y.J., Q.Z., H.C., J.M., J.D., and J. Li performed the analysis of 16S rRNA sequencing data and fecal metagenomic profiles. Y.J. analyzed the ultra-performance liquid chromatography-tandem mass spectrometry (UPLC-MS/MS) data. Y.J., J. Li, and X.-a.L. performed the statistical analysis and generated the figures and tables. H.C., Y.J., and Y.C. performed the clinical data analyses, which were overseen by Y.C., L.L., J. Liao, D.C., and X.-a.L. Y.J. and Q.Z. analyzed the animal experiment data, with Q.L., F.X., Z.C., and X.-a.L. providing oversight of the statistical analyses. Y.J., Z.C., and X.-a.L. prepared the manuscript. L.W., M.-H.H., and P.J.K. contributed to the revision of the manuscript. All authors approved the manuscript.

DECLARATION OF INTERESTS

The authors declare no competing interests.

STAR★METHODS

Detailed methods are provided in the online version of this paper and include the following:

- KEY RESOURCES TABLE
- EXPERIMENTAL MODEL AND STUDY PARTICIPANT DETAILS
  - Mice
  - Participants
- METHOD DETAILS
  - Bacteria
  - PTZ-induced seizures and behavioral seizure scoring
  - EEG implantation surgery
  - EEG recording and data analysis
  - Administration of BF839 and antibiotics
  - Microbial counting
  - 16S rRNA sequencing-based microbial profiling
  - Metagenomic sequencing and taxonomic profiling
  - Sparse labeling of hippocampal neurons
  - Golgi staining
  - UPLC-MS/MS
  - HPLC/MS analysis
  - Tissue dissection, immunofluorescence, and quantification
  - Colon viral injection
  - NG viral injection
  - Unilateral cervical vagotomy
  - Vagus nerve stimulation
  - Vagus nerve recording
  - Intrahippocampal kainic acid injection
  - Immunohistochemical analysis
  - Chemogenetic manipulation of the colonic ChAT$^+$–vagus nerve pathway
  - The co-cultivation of *B. fragilis* and *L. reuteri*
  - Metabolic predictions
  - Clinical observational study
- QUANTIFICATION AND STATISTICAL ANALYSIS
  - Statistical analyses
  - Image preparation

SUPPLEMENTAL INFORMATION

Supplemental information can be found online at https://doi.org/10.1016/j.neuron.2025.11.029.

Received: January 30, 2025
Revised: October 7, 2025
Accepted: November 26, 2025

REFERENCES

1. Sondhi, V., Agarwala, A., Pandey, R.M., Chakrabarty, B., Jauhari, P., Lodha, R., Toteja, G.S., Sharma, S., Paul, V.K., Kossoff, E., and Gulati, S. (2020). Efficacy of ketogenic diet, modified Atkins diet, and low glycemic index therapy diet among children with drug-resistant epilepsy: a randomized clinical trial. JAMA Pediatr. *174*, 944–951. https://doi.org/10.1001/jamapediatrics.2020.2282.
2. Kanner, A.M., and Bicchi, M.M. (2022). Review of antiseizure medications for adults with epilepsy-reply. JAMA *328*, 681. https://doi.org/10.1001/jama.2022.10600.
3. Mao, X., Wang, X., Jin, M., Li, Q., Jia, J., Li, M., Zhou, H., Liu, Z., Jin, W., Zhao, Y., and Luo, Z. (2022). Critical involvement of lysyl oxidase in seizure-induced neuronal damage through ERK-Alox5-dependent ferroptosis and its therapeutic implications. Acta Pharm. Sin. B *12*, 3513–3528. https://doi.org/10.1016/j.apsb.2022.04.017.
4. Symonds, J.D., Elliott, K.S., Shetty, J., Armstrong, M., Brunklaus, A., Cutcutache, I., Diver, L.A., Dorris, L., Gardiner, S., Jollands, A., et al. (2021). Early childhood epilepsies: epidemiology, classification, aetiology, and socio-economic determinants. Brain *144*, 2879–2891. https://doi.org/10.1093/brain/awab162.
5. Pan, I., LoPresti, M.A., Clarke, D.F., and Lam, S. (2020). The effectiveness of medical and surgical treatment for children with refractory epilepsy. Neurosurgery *88*, E73–E82. https://doi.org/10.1093/neuros/nyaa307.
6. Jia, Y., Jin, S., Hu, K., Geng, L., Han, C., Kang, R., Pang, Y., Ling, E., Tan, E.K., Pan, Y., and Liu, W. (2021). Gut microbiome modulates *Drosophila* aggression through octopamine signaling. Nat. Commun. *12*, 2698. https://doi.org/10.1038/s41467-021-23041-y.

7. Clemente, J.C., Ursell, L.K., Parfrey, L.W., and Knight, R. (2012). The impact of the gut microbiota on human health: an integrative view. Cell *148*, 1258–1270. https://doi.org/10.1016/j.cell.2012.01.035.

8. Sommer, F., and Bäckhed, F. (2013). The gut microbiota–masters of host development and physiology. Nat. Rev. Microbiol. *11*, 227–238. https://doi.org/10.1038/nrmicro2974.

9. Wu, G., Xu, T., Zhao, N., Lam, Y.Y., Ding, X., Wei, D., Fan, J., Shi, Y., Li, X., Li, M., et al. (2024). A core microbiome signature as an indicator of health. Cell *187*, 6550–6565.e11. https://doi.org/10.1016/j.cell.2024.09.019.

10. Sharon, G., Cruz, N.J., Kang, D.W., Gandal, M.J., Wang, B., Kim, Y.M., Zink, E.M., Casey, C.P., Taylor, B.C., Lane, C.J., et al. (2019). Human gut microbiota from autism spectrum disorder promote behavioral symptoms in mice. Cell *177*, 1600–1618.e17. https://doi.org/10.1016/j.cell.2019.05.004.

11. Lum, G.R., Ha, S.M., Olson, C.A., Blencowe, M., Paramo, J., Reyes, B., Matsumoto, J.H., Yang, X., and Hsiao, E.Y. (2023). Ketogenic diet therapy for pediatric epilepsy is associated with alterations in the human gut microbiome that confer seizure resistance in mice. Cell Rep. *42*, 113521. https://doi.org/10.1016/j.celrep.2023.113521.

12. Cryan, J.F., O'Riordan, K.J., Sandhu, K., Peterson, V., and Dinan, T.G. (2020). The gut microbiome in neurological disorders. Lancet Neurol. *19*, 179–194. https://doi.org/10.1016/S1474-4422(19)30356-4.

13. Mengoni, F., Salari, V., Kosenkova, I., Tsenov, G., Donadelli, M., Malerba, G., Bertini, G., Del Gallo, F., and Fabene, P.F. (2021). Gut microbiota modulates seizure susceptibility. Epilepsia *62*, e153–e157. https://doi.org/10.1111/epi.17009.

14. Olson, C.A., Vuong, H.E., Yano, J.M., Liang, Q.Y., Nusbaum, D.J., and Hsiao, E.Y. (2018). The gut microbiota mediates the anti-seizure effects of the ketogenic diet. Cell *173*, 1728–1741.e13. https://doi.org/10.1016/j.cell.2018.04.027.

15. Castells-Nobau, A., Mayneris-Perxachs, J., and Fernández-Real, J.M. (2024). Unlocking the mind-gut connection: impact of human microbiome on cognition. Cell Host Microbe *32*, 1248–1263. https://doi.org/10.1016/j.chom.2024.07.019.

16. Berryman, M.A., Milletich, P.L., Petrone, J.R., Roesch, L.F., Ilonen, J., Triplett, E.W., and Ludvigsson, J. (2022). Autoimmune-associated genetics impact probiotic colonization of the infant gut. J. Autoimmun. *133*, 102943. https://doi.org/10.1016/j.jaut.2022.102943.

17. Yang, J., Peng, M., Tan, S., Ge, S., Xie, L., Zhou, T., Liu, W., Zhang, K., Zhang, Z., Liu, J., and Shi, J. (2023). Calcium tungstate microgel enhances the delivery and colonization of probiotics during colitis via intestinal ecological niche occupancy. ACS Cent. Sci. *9*, 1327–1341. https://doi.org/10.1021/acscentsci.3c00227.

18. Jensen, B.A.H., Heyndrickx, M., Jonkers, D., Mackie, A., Millet, S., Naghibi, M., Pærregaard, S.I., Pot, B., Saulnier, D., Sina, C., et al. (2023). Small intestine vs. colon ecology and physiology: Why it matters in probiotic administration. Cell Rep. Med. *4*, 101190. https://doi.org/10.1016/j.xcrm.2023.101190.

19. Picciotto, M.R., Higley, M.J., and Mineur, Y.S. (2012). Acetylcholine as a neuromodulator: cholinergic signaling shapes nervous system function and behavior. Neuron *76*, 116–129. https://doi.org/10.1016/j.neuron.2012.08.036.

20. Nguyen, Q.A., Klein, P.M., Xie, C., Benthall, K.N., Iafrati, J., Homidan, J., Bendor, J.T., Dudok, B., Farrell, J.S., Gschwind, T., et al. (2024). Acetylcholine receptor based chemogenetics engineered for neuronal inhibition and seizure control assessed in mice. Nat. Commun. *15*, 601. https://doi.org/10.1038/s41467-024-44853-8.

21. Becchetti, A., Grandi, L.C., Cerina, M., and Amadeo, A. (2023). Nicotinic acetylcholine receptors and epilepsy. Pharmacol. Res. *189*, 106698. https://doi.org/10.1016/j.phrs.2023.106698.

22. Wang, Y., Wang, Y., Xu, C., Wang, S., Tan, N., Chen, C., Chen, L., Wu, X., Fei, F., Cheng, H., et al. (2020). Direct septum-hippocampus cholinergic circuit attenuates seizure through driving somatostatin inhibition. Biol. Psychiatry *87*, 843–856. https://doi.org/10.1016/j.biopsych.2019.11.014.

23. Kang, W.K., Florman, J.T., Araya, A., Fox, B.W., Thackeray, A., Schroeder, F.C., Walhout, A.J.M., and Alkema, M.J. (2024). Vitamin B12 produced by gut bacteria modulates cholinergic signalling. Nat. Cell Biol. *26*, 72–85. https://doi.org/10.1038/s41556-023-01299-2.

24. Petsakou, A., Liu, Y., Liu, Y., Comjean, A., Hu, Y., and Perrimon, N. (2023). Cholinergic neurons trigger epithelial Ca^{2+} currents to heal the gut. Nature *623*, 122–131. https://doi.org/10.1038/s41586-023-06627-y.

25. Suez, J., Zmora, N., Segal, E., and Elinav, E. (2019). The pros, cons, and many unknowns of probiotics. Nat. Med. *25*, 716–729. https://doi.org/10.1038/s41591-019-0439-x.

26. Whelan, K., Alexander, M., Gaiani, C., Lunken, G., Holmes, A., Staudacher, H.M., Theis, S., and Marco, M.L. (2024). Design and reporting of prebiotic and probiotic clinical trials in the context of diet and the gut microbiome. Nat. Microbiol. *9*, 2785–2794. https://doi.org/10.1038/s41564-024-01831-6.

27. Bialer, M., and White, H.S. (2010). Key factors in the discovery and development of new antiepileptic drugs. Nat. Rev. Drug Discov. *9*, 68–82. https://doi.org/10.1038/nrd2997.

28. Yang, Y., Tian, X., Xu, D., Zheng, F., Lu, X., Zhang, Y., Ma, Y., Li, Y., Xu, X., Zhu, B., and Wang, X. (2018). GPR40 modulates epileptic seizure and NMDA receptor function. Sci. Adv. *4*, eaau2357. https://doi.org/10.1126/sciadv.aau2357.

29. Dahlin, M., and Prast-Nielsen, S. (2019). The gut microbiome and epilepsy. eBioMedicine *44*, 741–746. https://doi.org/10.1016/j.ebiom.2019.05.024.

30. Geng, Z., Wang, X., Wu, F., Cao, Z., and Liu, J. (2023). Biointerface mineralization generates ultraresistant gut microbes as oral biotherapeutics. Sci. Adv. *9*, eade0997. https://doi.org/10.1126/sciadv.ade0997.

31. Casterline, B.W., Hecht, A.L., Choi, V.M., and Bubeck Wardenburg, J. (2017). The *Bacteroides fragilis* pathogenicity island links virulence and strain competition. Gut Microbes *8*, 374–383. https://doi.org/10.1080/19490976.2017.1290758.

32. Zhang, W., Zhu, B., Xu, J., Liu, Y., Qiu, E., Li, Z., Li, Z., He, Y., Zhou, H., Bai, Y., and Zhi, F. (2018). *Bacteroides fragilis* protects against antibiotic-associated diarrhea in rats by modulating intestinal defenses. Front. Immunol. *9*, 1040. https://doi.org/10.3389/fimmu.2018.01040.

33. Wexler, H.M. (2007). *Bacteroides*: the good, the bad, and the nitty-gritty. Clin. Microbiol. Rev. *20*, 593–621. https://doi.org/10.1128/CMR.00008-07.

34. Rosenberg, E.C., Chamberland, S., Bazelot, M., Nebet, E.R., Wang, X., McKenzie, S., Jain, S., Greenhill, S., Wilson, M., Marley, N., et al. (2023). Cannabidiol modulates excitatory-inhibitory ratio to counter hippocampal hyperactivity. Neuron *111*, 1282–1300.e8. https://doi.org/10.1016/j.neuron.2023.01.018.

35. Choy, M., Dadgar-Kiani, E., Cron, G.O., Duffy, B.A., Schmid, F., Edelman, B.J., Asaad, M., Chan, R.W., Vahdat, S., and Lee, J.H. (2022). Repeated hippocampal seizures lead to brain-wide reorganization of circuits and seizure propagation pathways. Neuron *110*, 221–236.e4. https://doi.org/10.1016/j.neuron.2021.10.010.

36. Taylor, J.A., Rodgers, K.M., Bercum, F.M., Booth, C.J., Dudek, F.E., and Barth, D.S. (2017). Voluntary control of epileptiform spike-wave discharges in awake rats. J. Neurosci. *37*, 5861–5869. https://doi.org/10.1523/jneurosci.3235-16.2017.

37. Kumari, S., and Brewster, A.L. (2024). Exploring dendritic and spine structural profiles in epilepsy: insights from human studies and experimental animal models. Epilepsy Curr. *24*, 40–46. https://doi.org/10.1177/15357597231218603.

38. Snigdha, S., Ha, K., Tsai, P., Dinan, T.G., Bartos, J.D., and Shahid, M. (2022). Probiotics: potential novel therapeutics for microbiota-gut-brain axis dysfunction across gender and lifespan. Pharmacol. Ther. *231*, 107978. https://doi.org/10.1016/j.pharmthera.2021.107978.

39. Waise, T.M.Z., Dranse, H.J., and Lam, T.K.T. (2018). The metabolic role of vagal afferent innervation. Nat. Rev. Gastroenterol. Hepatol. *15*, 625–636. https://doi.org/10.1038/s41575-018-0062-1.

40. Kaur, S., Selden, N.R., and Aballay, A. (2023). Anti-inflammatory effects of vagus nerve stimulation in pediatric patients with epilepsy. Front. Immunol. *14*, 1093574. https://doi.org/10.3389/fimmu.2023.1093574.

41. Jain, P., and Arya, R. (2021). Vagus nerve stimulation and seizure outcomes in pediatric refractory epilepsy: systematic review and meta-analysis. Neurology *96*, 1041–1051. https://doi.org/10.1212/WNL.0000000000012030.

42. Dawson, J., Abdul-Rahim, A.H., and Kimberley, T.J. (2024). Neurostimulation for treatment of post-stroke impairments. Nat. Rev. Neurol. *20*, 259–268. https://doi.org/10.1038/s41582-024-00953-z.

43. Stumpp, L., Smets, H., Vespa, S., Cury, J., Doguet, P., Delbeke, J., Nonclercq, A., and El Tahry, R. (2021). Vagus nerve electroneurogram-based detection of acute pentylenetetrazol induced seizures in rats. Int. J. Neural Syst. *31*, 2150024. https://doi.org/10.1142/S0129065721500246.

44. Bowles, S., Hickman, J., Peng, X., Williamson, W.R., Huang, R., Washington, K., Donegan, D., and Welle, C.G. (2022). Vagus nerve stimulation drives selective circuit modulation through cholinergic reinforcement. Neuron *110*, 2867–2885.e7. https://doi.org/10.1016/j.neuron.2022.06.017.

45. Kloc, M.L., Holmes, G.L., and Barry, J.M. (2024). Sex differences in cholinergic signaling affect functional outcomes for theta-gamma coordination in hippocampal subcircuits following experimental febrile status epilepticus. Epilepsia *65*, 2138–2151. https://doi.org/10.1111/epi.18017.

46. Friedman, A., Behrens, C.J., and Heinemann, U. (2007). Cholinergic dysfunction in temporal lobe epilepsy. Epilepsia *48*, 126–130. https://doi.org/10.1111/j.1528-1167.2007.01300.x.

47. Ndjim, M., Gasmi, I., Herbert, F., Joséphine, C., Bas, J., Lamrani, A., Coutry, N., Henry, S., Zimmermann, V.S., Dardalhon, V., et al. (2024). Tuft cell acetylcholine is released into the gut lumen to promote anti-helminth immunity. Immunity *57*, 1260–1273.e7. https://doi.org/10.1016/j.immuni.2024.04.018.

48. Randlett, O., Wee, C.L., Naumann, E.A., Nnaemeka, O., Schoppik, D., Fitzgerald, J.E., Portugues, R., Lacoste, A.M.B., Riegler, C., Engert, F., and Schier, A.F. (2015). Whole-brain activity mapping onto a zebrafish brain atlas. Nat. Methods *12*, 1039–1046. https://doi.org/10.1038/nmeth.3581.

49. Jameson, K.G., Kazmi, S.A., Ohara, T.E., Son, C., Yu, K.B., Mazdeyasnan, D., Leshan, E., Vuong, H.E., Paramo, J., Lopez-Romero, A., et al. (2025). Select microbial metabolites in the small intestinal lumen regulate vagal activity via receptor-mediated signaling. iScience *28*, 111699. https://doi.org/10.1016/j.isci.2024.111699.

50. Simon, G.L., and Gorbach, S.L. (1984). Intestinal flora in health and disease. Gastroenterology *86*, 174–193. https://doi.org/10.1016/0016-5085(84)90606-1.

51. Rode, J., Brengesjö Johnson, L., König, J., Rangel, I., Engstrand, L., Repsilber, D., and Brummer, R.J. (2024). Fecal samples and rectal swabs adequately reflect the human colonic luminal microbiota. Gut Microbes *16*, 2416912. https://doi.org/10.1080/19490976.2024.2416912.

52. Drokhlyansky, E., Smillie, C.S., Van Wittenberghe, N., Ericsson, M., Griffin, G.K., Eraslan, G., Dionne, D., Cuoco, M.S., Goder-Reiser, M.N., Sharova, T., et al. (2020). The human and mouse enteric nervous system at single-cell resolution. Cell *182*, 1606–1622.e23. https://doi.org/10.1016/j.cell.2020.08.003.

53. Širvinskas, D., Omrani, O., Lu, J., Rasa, M., Krepelova, A., Adam, L., Kaeppel, S., Sommer, F., and Neri, F. (2022). Single-cell atlas of the aging mouse colon. iScience *25*, 104202. https://doi.org/10.1016/j.isci.2022.104202.

54. Billipp, T.E., Fung, C., Webeck, L.M., Sargent, D.B., Gologorsky, M.B., Chen, Z., McDaniel, M.M., Kasal, D.N., McGinty, J.W., Barrow, K.A., et al. (2024). Tuft cell-derived acetylcholine promotes epithelial chloride secretion and intestinal helminth clearance. Immunity *57*, 1243–1259.e8. https://doi.org/10.1016/j.immuni.2024.03.023.

55. Kupari, J., Häring, M., Agirre, E., Castelo-Branco, G., and Ernfors, P. (2019). An atlas of vagal sensory neurons and their molecular specialization. Cell Rep. *27*, 2508–2523.e4. https://doi.org/10.1016/j.celrep.2019.04.096.

56. Kaelberer, M.M., Rupprecht, L.E., Liu, W.W., Weng, P., and Bohórquez, D.V. (2020). Neuropod cells: the emerging biology of gut-brain sensory transduction. Annu. Rev. Neurosci. *43*, 337–353. https://doi.org/10.1146/annurev-neuro-091619-022657.

57. Kaelberer, M.M., Buchanan, K.L., Klein, M.E., Barth, B.B., Montoya, M.M., Shen, X., and Bohórquez, D.V. (2018). A gut-brain neural circuit for nutrient sensory transduction. Science *361*, eaat5236. https://doi.org/10.1126/science.aat5236.

58. Buchanan, K.L., Rupprecht, L.E., Kaelberer, M.M., Sahasrabudhe, A., Klein, M.E., Villalobos, J.A., Liu, W.W., Yang, A., Gelman, J., Park, S., et al. (2022). The preference for sugar over sweetener depends on a gut sensor cell. Nat. Neurosci. *25*, 191–200. https://doi.org/10.1038/s41593-021-00982-7.

59. Jia, J., Zheng, L., Ye, L., Chen, J., Shu, S., Xu, S., Bao, X., Xia, S., Liu, R., Xu, Y., and Zhang, M. (2023). CD11c^{+} microglia promote white matter repair after ischemic stroke. Cell Death Dis. *14*, 156. https://doi.org/10.1038/s41419-023-05689-0.

60. Ali, M.S.S., Parastooei, G., Raman, S., Mack, J., Kim, Y.S., and Chung, M.K. (2024). Genetic labeling of the nucleus of tractus solitarius neurons associated with electrical stimulation of the cervical or auricular vagus nerve in mice. Brain Stimul. *17*, 987–1000. https://doi.org/10.1016/j.brs.2024.08.007.

61. Okonogi, T., Kuga, N., Yamakawa, M., Kayama, T., Ikegaya, Y., and Sasaki, T. (2024). Stress-induced vagal activity influences anxiety-relevant prefrontal and amygdala neuronal oscillations in male mice. Nat. Commun. *15*, 183. https://doi.org/10.1038/s41467-023-44205-y.

62. Parker, A., Romano, S., Ansorge, R., Aboelnour, A., Le Gall, G., Savva, G.M., Pontifex, M.G., Telatin, A., Baker, D., Jones, E., et al. (2022). Fecal microbiota transfer between young and aged mice reverses hallmarks of the aging gut, eye, and brain. Microbiome *10*, 68. https://doi.org/10.1186/s40168-022-01243-w.

63. Diener, C., Gibbons, S.M., and Resendis-Antonio, O. (2020). MICOM: metagenome-scale modeling to infer metabolic interactions in the gut microbiota. mSystems *5*, e00606–e00619. https://doi.org/10.1128/mSystems.00606-19.

64. Ardalani, O., Phaneuf, P.V., Mohite, O.S., Nielsen, L.K., and Palsson, B.O. (2024). Pangenome reconstruction of Lactobacillaceae metabolism predicts species-specific metabolic traits. mSystems *9*, e0015624. https://doi.org/10.1128/msystems.00156-24.

65. Bloom, S.M., Mafunda, N.A., Woolston, B.M., Hayward, M.R., Frempong, J.F., Abai, A.B., Xu, J., Mitchell, A.J., Westergaard, X., Hussain, F.A., et al. (2022). Cysteine dependence of Lactobacillus iners is a potential therapeutic target for vaginal microbiota modulation. Nat. Microbiol. *7*, 434–450. https://doi.org/10.1038/s41564-022-01070-7.

66. Landete, J.M., García-Haro, L., Blasco, A., Manzanares, P., Berbegal, C., Monedero, V., and Zúñiga, M. (2010). Requirement of the Lactobacillus casei MaeKR two-component system for L-malic acid utilization via a malic enzyme pathway. Appl. Environ. Microbiol. *76*, 84–95. https://doi.org/10.1128/aem.02145-09.

67. Sharon, G., Sampson, T.R., Geschwind, D.H., and Mazmanian, S.K. (2016). The central nervous system and the gut microbiome. Cell *167*, 915–932. https://doi.org/10.1016/j.cell.2016.10.027.

68. Coley, E.J.L., and Hsiao, E.Y. (2021). Malnutrition and the microbiome as modifiers of early neurodevelopment. Trends Neurosci. *44*, 753–764. https://doi.org/10.1016/j.tins.2021.06.004.

69. Howitt, M.R., Lavoie, S., Michaud, M., Blum, A.M., Tran, S.V., Weinstock, J.V., Gallini, C.A., Redding, K., Margolskee, R.F., Osborne, L.C., et al. (2016). Tuft cells, taste-chemosensory cells, orchestrate parasite type 2 immunity in the gut. Science *351*, 1329–1333. https://doi.org/10.1126/science.aaf1648.

70. Parikh, K., Antanaviciute, A., Fawkner-Corbett, D., Jagielowicz, M., Aulicino, A., Lagerholm, C., Davis, S., Kinchen, J., Chen, H.H., Alham, N.K., et al. (2019). Colonic epithelial cell diversity in health and inflammatory bowel disease. Nature *567*, 49–55. https://doi.org/10.1038/s41586-019-0992-y.

71. Schneider, C., O'Leary, C.E., von Moltke, J., Liang, H.E., Ang, Q.Y., Turnbaugh, P.J., Radhakrishnan, S., Pellizzon, M., Ma, A., and Locksley, R.M. (2018). A Metabolite-Triggered Tuft Cell-ILC2 Circuit Drives Small Intestinal Remodeling. Cell *174*, 271–284.e14. https://doi.org/10.1016/j.cell.2018.05.014.

72. Gerbe, F., Sidot, E., Smyth, D.J., Ohmoto, M., Matsumoto, I., Dardalhon, V., Cesses, P., Garnier, L., Pouzolles, M., Brulin, B., et al. (2016). Intestinal epithelial tuft cells initiate type 2 mucosal immunity to helminth parasites. Nature *529*, 226–230. https://doi.org/10.1038/nature16527.

73. Cuesta, S., Burdisso, P., Segev, A., Kourrich, S., and Sperandio, V. (2022). Gut colonization by *Proteobacteria* alters host metabolism and modulates cocaine neurobehavioral responses. Cell Host Microbe *30*, 1615–1629.e5. https://doi.org/10.1016/j.chom.2022.09.014.

74. Parker, A., Fonseca, S., and Carding, S.R. (2020). Gut microbes and metabolites as modulators of blood-brain barrier integrity and brain health. Gut Microbes *11*, 135–157. https://doi.org/10.1080/19490976.2019.1638722.

75. Borre, Y.E., O'Keeffe, G.W., Clarke, G., Stanton, C., Dinan, T.G., and Cryan, J.F. (2014). Microbiota and neurodevelopmental windows: implications for brain disorders. Trends Mol. Med. *20*, 509–518. https://doi.org/10.1016/j.molmed.2014.05.002.

76. Schneider, E., O'Riordan, K.J., Clarke, G., and Cryan, J.F. (2024). Feeding gut microbes to nourish the brain: unravelling the diet-microbiota-gut-brain axis. Nat. Metab. *6*, 1454–1478. https://doi.org/10.1038/s42255-024-01108-6.

77. Tao, J., Campbell, J.N., Tsai, L.T., Wu, C., Liberles, S.D., and Lowell, B.B. (2021). Highly selective brain-to-gut communication via genetically defined vagus neurons. Neuron *109*, 2106–2115.e4. https://doi.org/10.1016/j.neuron.2021.05.004.

78. Schütz, B., Ruppert, A.L., Strobel, O., Lazarus, M., Urade, Y., Büchler, M.W., and Weihe, E. (2019). Distribution pattern and molecular signature of cholinergic tuft cells in human gastro-intestinal and pancreatic-biliary tract. Sci. Rep. *9*, 17466. https://doi.org/10.1038/s41598-019-53997-3.

79. Muise, E.D., Gandotra, N., Tackett, J.J., Bamdad, M.C., and Cowles, R.A. (2017). Distribution of muscarinic acetylcholine receptor subtypes in the murine small intestine. Life Sci. *169*, 6–10. https://doi.org/10.1016/j.lfs.2016.10.030.

80. Goldstein, N., McKnight, A.D., Carty, J.R.E., Arnold, M., Betley, J.N., and Alhadeff, A.L. (2021). Hypothalamic detection of macronutrients via multiple gut-brain pathways. Cell Metab. *33*, 676–687.e5. https://doi.org/10.1016/j.cmet.2020.12.018.

81. Rupprecht, L.E., and Bohórquez, D.V. (2021). The nerve not taken. Cell Metab. *33*, 466–467. https://doi.org/10.1016/j.cmet.2021.02.014.

82. Sahasrabudhe, A., Rupprecht, L.E., Orguc, S., Khudiyev, T., Tanaka, T., Sands, J., Zhu, W., Tabet, A., Manthey, M., Allen, H., et al. (2023). Multifunctional microelectronic fibers enable wireless modulation of gut and brain neural circuits. Nat. Biotechnol. *42*, 892–904. https://doi.org/10.1038/s41587-023-01833-5.

83. Tamana, S.K., Tun, H.M., Konya, T., Chari, R.S., Field, C.J., Guttman, D.S., Becker, A.B., Moraes, T.J., Turvey, S.E., Subbarao, P., et al. (2021). *Bacteroides*-dominant gut microbiome of late infancy is associated with enhanced neurodevelopment. Gut Microbes *13*, 1–17. https://doi.org/10.1080/19490976.2021.1930875.

84. Citraro, R., Lembo, F., De Caro, C., Tallarico, M., Coretti, L., Iannone, L.F., Leo, A., Palumbo, D., Cuomo, M., Buommino, E., et al. (2021). First evidence of altered microbiota and intestinal damage and their link to absence epilepsy in a genetic animal model, the WAG/Rij rat. Epilepsia *62*, 529–541. https://doi.org/10.1111/epi.16813.

85. Furuichi, M., Kawaguchi, T., Pust, M.M., Yasuma-Mitobe, K., Plichta, D.R., Hasegawa, N., Ohya, T., Bhattarai, S.K., Sasajima, S., Aoto, Y., et al. (2024). Commensal consortia decolonize *Enterobacteriaceae* via ecological control. Nature *633*, 878–886. https://doi.org/10.1038/s41586-024-07960-6.

86. Sanna, S., Kurilshikov, A., van der Graaf, A., Fu, J., and Zhernakova, A. (2022). Challenges and future directions for studying effects of host genetics on the gut microbiome. Nat. Genet. *54*, 100–106. https://doi.org/10.1038/s41588-021-00983-z.

87. Fisher, R.S., Cross, J.H., French, J.A., Higurashi, N., Hirsch, E., Jansen, F.E., Lagae, L., Moshé, S.L., Peltola, J., Roulet Perez, E., et al. (2017). Operational classification of seizure types by the International League Against Epilepsy: Position Paper of the ILAE Commission for Classification and Terminology. Epilepsia *58*, 522–530. https://doi.org/10.1111/epi.13670.

88. Zhong, H.J., Wang, S.Q., Zhang, R.X., Zhuang, Y.P., Li, L., Yi, S.Z., Li, Y., Wu, L., Ding, Y., Zhang, J., et al. (2023). Supplementation with high-GABA-producing *Lactobacillus plantarum L5* ameliorates essential tremor triggered by decreased gut bacteria-derived GABA. Transl. Neurodegener. *12*, 58. https://doi.org/10.1186/s40035-023-00391-9.

89. Zhu, H., Cao, C., Wu, Z., Zhang, H., Sun, Z., Wang, M., Xu, H., Zhao, Z., Wang, Y., Pei, G., et al. (2021). The probiotic L. casei Zhang slows the progression of acute and chronic kidney disease. Cell Metab. *33*, 2091–2093. https://doi.org/10.1016/j.cmet.2021.08.015.

90. Lin, R., Wang, R., Yuan, J., Feng, Q., Zhou, Y., Zeng, S., Ren, M., Jiang, S., Ni, H., Zhou, C., et al. (2018). Cell-type-specific and projection-specific brain-wide reconstruction of single neurons. Nat. Methods *15*, 1033–1036. https://doi.org/10.1038/s41592-018-0184-y.

91. Fowler, C.D., Lu, Q., Johnson, P.M., Marks, M.J., and Kenny, P.J. (2011). Habenular α5 nicotinic receptor subunit signalling controls nicotine intake. Nature *471*, 597–601. https://doi.org/10.1038/nature09797.

92. Mughrabi, I.T., Hickman, J., Jayaprakash, N., Thompson, D., Ahmed, U., Papadoyannis, E.S., Chang, Y.C., Abbas, A., Datta-Chaudhuri, T., Chang, E.H., et al. (2021). Development and characterization of a chronic implant mouse model for vagus nerve stimulation. eLife *10*, e61270. https://doi.org/10.7554/eLife.61270.

93. Fallon, I.P., Hughes, R.N., Severino, F.P.U., Kim, N., Lawry, C.M., Watson, G.D.R., Roshchina, M., and Yin, H.H. (2023). The role of the parafascicular thalamic nucleus in action initiation and steering. Curr. Biol. *33*, 2941–2951.e4. https://doi.org/10.1016/j.cub.2023.06.025.

94. Kang, W., Ju, C., Joo, J., Lee, J., Shon, Y.M., and Park, S.M. (2022). Closed-loop direct control of seizure focus in a rodent model of temporal lobe epilepsy via localized electric fields applied sequentially. Nat. Commun. *13*, 7805. https://doi.org/10.1038/s41467-022-35540-7.

95. Huang, Y.J., Hung, C.C., Hsu, P.C., Lee, P.Y., Tsai, Y.A., Hsin, Y.C., Lee, X.T., Chou, C.C., Chen, M.L., Tarng, D.C., and Lee, Y.H. (2023). Astrocytic aryl hydrocarbon receptor mediates chronic kidney disease-associated mental disorders involving GLT1 hypofunction and neuronal activity enhancement in the mouse brain. Glia *71*, 1057–1080. https://doi.org/10.1002/glia.24326.

96. Heinken, A., Hertel, J., Acharya, G., Ravcheev, D.A., Nyga, M., Okpala, O.E., Hogan, M., Magnúsdóttir, S., Martinelli, F., Nap, B., et al. (2023). Genome-scale metabolic reconstruction of 7,302 human microorganisms for personalized medicine. Nat. Biotechnol. *41*, 1320–1331. https://doi.org/10.1038/s41587-022-01628-0.

97. El-Sharkawy, O.S., El-Rashidy, O.F., Elagouza, I.A.A., Nassar, B.A., and Taha, S.I. (2024). The beneficial effect of probiotics as an adjuvant treatment in childhood drug resistant epilepsy: a prospective pilot study. Int. J. Immunopathol. Pharmacol. *38*, 3946320241291276. https://doi.org/10.1177/03946320241291276.

98. Nabbout, R., Mistry, A., Zuberi, S., Villeneuve, N., Gil-Nagel, A., Sanchez-Carpintero, R., Stephani, U., Laux, L., Wirrell, E., Knupp, K., et al. (2020). Fenfluramine for treatment-resistant seizures in patients with Dravet syndrome receiving stiripentol-inclusive regimens: a randomized clinical trial. JAMA Neurol. *77*, 300–308. https://doi.org/10.1001/jamaneurol.2019.4113.

Please cite this article in press as: Jia et al., Gut-brain cholinergic signaling mediates the antiseizure effects of *Bacteroides fragilis*, Neuron (2025), https://doi.org/10.1016/j.neuron.2025.11.029

STAR★METHODS

KEY RESOURCES TABLE

REAGENT or RESOURCE	SOURCE	IDENTIFIER
Antibodies		
Rabbit anti-ZO1 tight junction protein polyclonal antibody	abcam	Cat# ab216880; RRID: AB_2909434
Rabbit anti-Occludin polyclonal antibody	abcam	Cat# ab222691; RRID: AB_222691
Rabbit anti-c-Fos monoclonal antibody	Abclonal	Cat# A24620; RRID: AB_3677371
Mouse anti-ChAT monoclonal antibody	Thermo Fisher Scientific	Cat# MA5-31383; RRID: AB_2787020
Rabbit anti-PGP9.5	Proteintech	Cat# 14730-1-AP; RRID: AB_2210497
Chicken anti-GFP polyclonal antibody	Abcam	Cat# ab13970; RRID: AB_300798
Chicken anti-mCherry polyclonal antibody	Abcam	Cat# ab205402; RRID: AB_2722769
Rabbit anti-tyrosine hydroxylase polyclonal antibody	Millipore	Cat# AB152; RRID: AB_390204
Mouse anti-pERK1 monoclonal antibody	Cell signaling	Cat# 4370; RRID: AB_2315112
Rabbit synapsin 1 monoclonal antibody	Cell Signaling	Cat# 5297; RRID: AB_2616578
Anti-rabbit IgG, HRP-linked Antibody	Cell Signaling	Cat# 7074P2; RRID: AB_2099233
Alexa Fluor® 488 AffiniPure Fab Fragment Goat Anti-Rabbit IgG (H+L)	Jackson ImmunoResearch Labs	Cat# 111-547-003; RRID: AB_2338058
Alexa Fluor® 488 Goat Anti-Chicken IgY preadsorbed (H+L)	Abcam	Cat# ab150173; RRID: AB_2827653
Alexa Fluor® 594 Goat Anti-Chicken IgY preadsorbed (H+L)	Abcam	Cat# ab150176; RRID: AB_2716250
Alexa Fluor® 594 AffiniPure Goat Anti-Mouse IgG (H+L)	Jackson ImmunoResearch Labs	Cat# 115-585-003; RRID: AB_2338871
Bacterial and virus strains		
rAAV-NCSP-YFP-2E5	Brain Case	Cat# SL001
AAV9-Retro-CAG-EGFP	Brain Case	Cat# BC-0251
PRV-CAG-EGFP	Brain Case	Cat# BC-PRV-531-Pro
AAV-ChAT-DIO-EGFP	Brain Case	Cat# BC-0424
AAV-ChAT-DIO-hM3Dq-EGFP	Brain Case	Cat# BC-4404
AAV-ChAT-DIO-taCasp3-TEVp-EGFP	Brain Case	Cat# BC-4405
RV-EnvA-ΔG-mCherry-Cre	Brain Case	Cat# BC-RV-CVSEnvA472
AAV-hSyn-TVA	Brain Case	Cat# BC-2042
AAV-hSyn-N2cG	Brain Case	Cat# BC-4406
Lactobacillus reuteri	This paper	GenBank: OR771366.1
Bacteroides fragile 839	Guangzhou Totem Life Medical Research Company	N/A
Lactobacillus rhamnosus TT628	Guangzhou Totem Life Medical Research Company	N/A
Placebo	Guangzhou Totem Life Medical Research Company	N/A
Chemicals, peptides, and recombinant proteins		
Citrate retrieval	Zytomed	Cat# ZUC028-500
Frozen Section Neuron Golgi Staining Kit	Genmed	Cat# GMS80020.1
DL-Adrenalin	Acmec Biochemical	Cat# D60240-1g
Taurine	Solarbio	Cat# ST8410
Nicotinic acid	Solarbio	Cat# N8060
5-hydroxytryptamine hydrochloride	Solarbio	Cat# S9740

(*Continued on next page*)

Please cite this article in press as: Jia et al., Gut-brain cholinergic signaling mediates the antiseizure effects of *Bacteroides fragilis*, Neuron (2025), https://doi.org/10.1016/j.neuron.2025.11.029

Continued

REAGENT or RESOURCE	SOURCE	IDENTIFIER
γ- aminobutyric acid	Solarbio	Cat# SA8240
Dopamine hydrochloride	Solarbio	Cat# SD8600
L-glutamate	Solarbio	Cat# G0010
Kainic acid	Solarbio	Cat# IK1000
Norepinephrine	Shyuanye	Cat# B24713
2-Hydroxy-N,N,N-Trimethyl-Ethanaminium(Choline)	Shyuanye	Cat# T25208
Pentylenetetrazole	Sigma	Cat# P6500
dNTPmix10mM	Invitrogen	Cat# 18-427-088
Vancomycine	Dalian Meilun Biotechnology	Cat# MB1260
Streptomycin	Macklin	Cat# S875203
Neomycin	Macklin	Cat# N6063
Gentamycin	OXOID	Cat# CT0695B
Lidocaine	Aladdin	Cat# L129221
Acetylcholine Chloride	ApexBio Technology	Cat# B1596
Mecamylamine hydrochloride	ApexBio Technology	Cat# B7205
Bupivacaine	Acmec Biochemical	Cat# B75920
DAPI	Solarbio	Cat# C0060
Fluoro-Gold	KEYGEN BIOTECH	Cat# KGMP023
Deschloroclozapine	MedChemExpress	Cat# HY-42110
Normal goat serum	Beyotime	Cat# C0265
Critical commercial assays		
Modified gifu anaerobic medium broth medium	Haibo Company	Cat# HB8518-3
Nutrient medium	Haibo Company	Cat# HB0109
M.R.S. medium	Haibo Company	Cat# HB0384
Experimental models: Organisms/strains		
C57BL/6J mice	Hunan SJA Laboratory Animal	N/A
Software and algorithms		
Graph-Pad Prism software, version 8.0	Graphpad	https://www.graphpad.com/
Origin 2024	OriginLab	https://www.originlab.com/
Fiji Image J	Fiji	https://fiji.sc/
MATLAB 2019b	MATLAB	https://ww2.mathworks.cn/products/matlab.html
RIGOL DHO800 system	RIGOL Technologies	https://www.rigol.com/products/detail/DHO800
SCIEX OS-MQ software	Danaher Life Sciences	https://sciex.com.cn/products/software/sciex-os-software
Adobe Illustrator 2020	Adobe	https://www.adobe.com/cn/products/illustrator.html
Apollo II high-throughput neural recording system	Originopto Biotechnology	https://bio-signal.com/?list_19/38.html
Neuroexplorer software	Nex Technologies	https://www.neuroexplorer.com/
Imaris Viewer	OXFORD instruments	https://imaris.oxinst.com/imaris-viewer
USEARCH software	USEARCH	https://www.drive5.com/usearch/

EXPERIMENTAL MODEL AND STUDY PARTICIPANT DETAILS

Mice

All experiments in mice were performed after approval by the Institutional Animal Care and Use Committee of the Shenzhen Institutes of Advanced Technology, Chinese Academy of Sciences (SIAT-IACUC-220901-NS-LXA-A2184). Male C57BL/6J mice, aged

3 weeks, were housed in groups under standard conditions with a 12/12 h day/night cycle (lights on at 7 am and off at 7 pm) with ad libitum access to water and standard mouse chow (Purina 5001). Mice were randomly assigned to experimental groups. Experiments included age-matched cohorts of males.

Participants

NDPE observational microbiome cohort (cohort 1)

Cohort 1 comprised 114 pediatric patients with newly diagnosed pediatric epilepsy (NDPE) and 63 age- and sex-matched healthy controls recruited at Shenzhen Children's Hospital (Ethics Approval No. 202212403). NDPE was diagnosed according to the 2017 International League Against Epilepsy (ILAE) classification.[87] Eligible participants were (1) aged 1–14 years and (2) newly diagnosed and treated at Shenzhen Children's Hospital following the first occurrence of epileptic symptoms. Exclusion criteria included (1) intracranial space-occupying lesions, malformations, or other surgically resectable abnormalities; (2) comorbidities that could interfere with study assessments; (3) severe cardiac, hepatic, or renal dysfunction; (4) anticipated inability to complete regular follow-up assessments; and (5) participation in other clinical trials. Healthy controls were included if they (1) were 1–14 years old; (2) had no history of neurological, metabolic, gastrointestinal, or chronic systemic diseases; and (3) had not used antibiotics, probiotics, or ketogenic diet within the preceding month. Control exclusion criteria included any acute or chronic illness or medication exposure that could affect gut microbiota composition.

Refractory epilepsy metagenomic profiling cohort (cohort 2)

Cohort 2 included 37 pediatric patients with refractory epilepsy recruited from Shenzhen Children's Hospital (Ethics Approval No. 202212403), while age- and sex-matched healthy control metagenomic data were obtained from the China National Center for Bioinformation (CNCB; BioProject: PRJCA001532, n = 39). Refractory epilepsy was diagnosed according to the 2017 ILAE criteria. Eligible participants (1) were 1–14 years old; (2) had failed to achieve seizure control despite treatment with at least two appropriate antiseizure medications and had not responded to other therapeutic modalities, including neurostimulation, additional medications, or surgery; (3) had experienced at least one seizure every four weeks during the eight weeks preceding screening; (4) had been on stable therapeutic regimens for at least four weeks before screening and were expected to maintain stability during the study; and (5) experienced at least one seizure during the four-week baseline observation period. Exclusion criteria included intracranial structural abnormalities, comorbidities that could interfere with study assessments, severe cardiac, hepatic, or renal dysfunction, inability to complete scheduled follow-up visits, or participation in other clinical studies.

BF839 randomized controlled trial (cohort 3)

Cohort 3 was approved by the Medical Ethics Committee of Shenzhen Children's Hospital (Approval No. 202007502) and registered with the Chinese Clinical Trial Registry (Registration No. ChiCTR2100042203). This cohort included pediatric patients with refractory epilepsy who met the same diagnostic and screening criteria as those in cohort 2. Eligible participants were randomly assigned (1:1) to receive either BF839 or a placebo. Participants were excluded if they (1) had received ketogenic diet therapy, antibiotics, or other probiotic treatments within one month prior to screening; (2) had intracranial space-occupying lesions, malformations, or other surgically resectable abnormalities; (3) had comorbidities that could interfere with study assessments; (4) had severe cardiac, hepatic, or renal dysfunction; (5) were expected to be unable to complete scheduled follow-up evaluations; (6) were participating in other clinical trials; or (7) were unable to take oral medication, including those requiring gastrostomy tube feeding or other enteral administration routes. Withdrawal criteria included (1) failure to adhere to the study treatment; (2) the need for major adjustments to antiseizure medications due to a significant increase in seizure frequency; (3) the occurrence of severe adverse reactions; or (4) withdrawal at the request of parents or legal guardians. Additional methodological details are provided in the Trial Protocol.

Written informed consent was obtained from all participants or their legal guardians. Fecal samples were collected across all three cohorts. In cohorts 1 and 2, samples were collected during each participant's initial hospital visit and immediately stored at –80°C until processing. In cohort 3, samples were collected at baseline and again three months after BF839 or placebo administration. To support adequate nutrition and minimize potential seizure triggers, personalized daily dietary guidelines were provided to participants in cohort 3, avoiding foods such as those containing caffeine or spicy ingredients. 16S rRNA gene sequencing was performed for cohorts 1 and 3, whereas cohort 2 underwent whole-genome shotgun metagenomic sequencing. Participant characteristics are summarized in Tables S1, S2, and S3.

METHOD DETAILS

Bacteria

BF839 is a non-toxigenic strain of *B. fragilis*, originally isolated in 1983 from the feces of healthy, well-nourished infants during a study on normal gut microbiota conducted by Zhang J.J. Based on comprehensive microbiological characterization, functional analyses, and clinical observations, the strain was identified as a beneficial human commensal and designated BF839 by Zhang J.J. in 1991. In this study, BF839 was gifted by the Dalian Totem Biological Engineering Co., Ltd. (Originally known as: Dalian Totem Biological Engineering Research Institute) as a purified bacterial isolate, rather than a commercial probiotic mixture. The product underwent quality control testing including 16S rRNA sequencing and viable count assessments prior to use in our experiments. The viable probiotic bacteria were at least 10^8 CFU/g.

For bacterial culture experiments, BF839 was cultured under anaerobic conditions at 37°C in modified Gifu anaerobic medium (GAM). *L. reuteri* was cultured anaerobically at 37°C in MRS (de Man, Rogosa, Sharpe) medium, with a pH value of 6.0. Cultures were authenticated by full-length 16S rRNA sequencing.

PTZ-induced seizures and behavioral seizure scoring

All experiments were performed between 9:00 and 12:00. The PTZ-induced seizure model was performed as previously described. Briefly, 3 mg/mL PTZ was dissolved in sterile 0.9% (w/v) NaCl, followed by intraperitoneal injection of PTZ with a 1 ml syringe every other day for a total of 12 injections. To ensure unbiased behavioral assessment, all treatment groups (including control and experimental cohorts) were assigned random three-digit codes by an independent researcher not involved in data acquisition or analysis.

Mice were placed in an observation chamber for habituation. During the habituation period (3 min), the volume of PTZ solution for injection was calculated based on the animal's body weight and the 30 mg/kg PTZ injection dose. The video recording equipment was calibrated to exclude group identifiers from the captured footage. Seizure-related behaviors were monitored via continuous video recording for 30 min following PTZ administration. For blinded behavioral scoring, all video files were anonymized and renamed using a randomized coding algorithm to eliminate temporal or group-related identifiers. Two certified epileptologists (each with >5 years of clinical and experimental experience in seizure classification) independently evaluated the anonymized recordings. Prior to scoring, both raters completed standardized calibration using a curated set of reference videos from our laboratory, achieving a Cohen's κ of 0.85 in pre-study inter-rater reliability assessment. Group assignment remained concealed until the completion of statistical analyses. Seizure severity was assessed using a modified Racine scale adapted for PTZ-induced seizures, consisting of five discrete stages: 1) myoclonic jerks, 2) head stereotypy and facial clonus, 3) bilateral and alternating forelimb/hindlimb clonus, 4) rearing and falling, and 5) generalized tonic-clonic episodes. The mean seizure score for each mouse was calculated from the seizure severity scores recorded during all 11 PTZ-induced seizures. Scoring discrepancies exceeding one stage between raters were resolved by consensus review with a third independent neurologist, blinded to treatment conditions.

EEG implantation surgery

Mice were anesthetised with isoflurane, placed on a homeothermic blanket and ophthalmic ointment applied. The fur was removed along the head and the area cleaned with sterile saline, 75% ethanol and iodophor. Using sterile surgical instruments, a 2 cm incision was made along the dorsal midline from the posterior eye margin to a point midway between the shoulder blades. The mice were positioned in a stereotaxic instrument and 1 mg/kg lidocaine + 1 mg/kg bupivacaine was applied locally along the incision site. The skull was cleaned with sterile saline, 75% ethanol and iodophor. Using a 1.0 mm microdrill, the skull was perforated to provide three small holes for implantation of three subdural electrodes (1 recording, 1 reference, 1 ground). The recording hole was drilled over the right hippocampus (1.8 mm A-P, + 1.1 mm M-L) and the reference burr hole was drilled anterior to the recording hole (-1.5 mm A-P, -1.5 mm M-L) to serve as cortical recording leads. Unilateral EEG recording electrodes (0.10″ length stainless steel) were implanted epidurally over the frontoparietal cortex. Sterile acrylic was applied to the dried area. The burr hole was drilled over the cerebellar region (5.7 mm A-P, 1.25 mm M-L). The subdural screw electrodes were attached to a 3-pin connector (Xinhongnuo Electronics Co., Ltd, Shenzhen, China), which was fixed to the skull with sterile acrylic.

EEG recording and data analysis

After EEG implantation surgery, the mice were acclimated to the recording environment in the room where the vEEG equipment was located. EEGs were recorded after the 12th PTZ injection. During EEG recording, the animals were allowed to move freely and had access to food and water. A pre-amplifier (Solar Electronic Technology Co., Ltd, Beijing, China) was connected to the 3-pin connector and then to a commutator (Solar Electronic Technology Co., Ltd, Beijing, China). PTZ (30 mg/kg, intraperitoneally) was then injected. EEG signals were amplified 10-fold and recorded at 2 kHz sampling rate using a bandpass filter (0.5-500 Hz) and Solar Acquisition System (Solar Electronic Technology Co., Ltd, Beijing, China). Simultaneously, high frame rate video (30 fs) was recorded using an infrared LED camera (DAHUA Technology Co., Ltd, Hangzhou, China). Seizures were identified on the basis of characteristic spike patterns in 5 stages: A) low-frequency background with low-voltage spikes, B) synchronized high-frequency, high-voltage spikes, C) high-frequency, low-voltage spikes, D) unsynchronized high-frequency, high-voltage spikes, and E) high-frequency, burst spikes. Data were analyzed by a blinded researcher using MATLAB 2019 software. EEG signals were filtered with a 10 Hz high-pass filter, and seizure events were detected by blinded manual scoring. Seizures were defined as patterns of high-frequency, high-voltage synchronized heterogeneous spike waveforms with amplitudes at least two times greater than background and lasting more than 6 s. Average spike frequency per seizure was determined as the number of spikes above baseline per second in a given seizure and averaged per animal.

Administration of BF839 and antibiotics

Mice were pretreated with BF839 (1 x 10^9 CFU/day) by gavage for one week, followed by the PTZ-induced seizure model and continuously treated with BF839 until the mice were sacrificed. Antibiotics were administered ad libitum in the drinking water and replaced every other day with a freshly prepared solution, similar to that described above, containing vancomycin (500 μg/ml), streptomycin (50 μg/ml), neomycin (100 μg/ml) and gentamycin (100 μg/ml) (mice were treated for one week). Mice were housed in cages and pretreated with antibiotics for 3 days. After this pretreatment, BF839 was administered to them by gavage at a dose of 1 x 10^9 CFU per

Please cite this article in press as: Jia et al., Gut-brain cholinergic signaling mediates the antiseizure effects of *Bacteroides fragilis*, Neuron (2025), https://doi.org/10.1016/j.neuron.2025.11.029

day. Subsequently, the mice were treated with PTZ to induce seizures. Pilot studies showed no significant differences in fecal DNA concentration or 16S rRNA amplification (indicators associated with bacterial load) between colonization groups.

Microbial counting

Lactobacillus were identified and counted by plate colony-counting method used M.R.S. plates.[88] In brief, after the 12th PTZ injection and different bacteria gavaged, 1g of fresh mice feces from each group were placed in 200 μl of sterile physiological saline in a 1.5-ml screw-top microcentrifuge tube. Samples were homogenized for 2 min at 8000r/min, and then spin down 30 s at 1000 rpm and take out supernatants. The seven 1/10 dilutions for the supernatants were made and plated on M.R.S at 37°C under anaerobic conditions. Three randomly selected colonies in the plate were identified by 16S rRNA gene PCR with using primers 338F (5'-ACTCCTACGGGAGGCAGC-3') and 806R (5'- GGACTACHVGGGTWTCTAAT-3'). 16S rRNA gene sequence data was characterized by BLAST analysis.

16S rRNA sequencing-based microbial profiling

Fecal samples from each mouse were collected and sent to Oebiotech Biomedical Technology Co., Ltd (Shanghai, China). Total bacterial DNA extraction and sequencing was performed according to standard protocols.[89] Briefly, the hypervariable regionV3&V4 of bacterial 16S rRNA gene were captured using the Illumina Nextera protocol and a single amplicon of about 460 bp was amplified as described in the Illumina protocol. The PCR product was cleaned using Agencourt AmpureXP beads from Beckman Coulter Genomics. Illumina adaptor and barcode sequences were ligated to the amplicons in order to attach them to MiSeqDx flow cell and for multiplexing. Quality and quantity of each sequencing library was assessed using Bioanlyzer and PicoGreen measurements, respectively. About 6 pM of pooled libraries was loaded onto a MiSeqDX flow cell and sequenced using PE300 (Paired end 300 bp) v3 kit. Raw fastq files were demultiplexed based on unique barcodes and assessed for quality. Samples with more than 50 K QC pass sequencing reads were used for downstream 16S operational taxonomic units (OTU) analysis. OTU were selected using the de novo OTU picking protocol with a 97% similarity threshold.

Metagenomic sequencing and taxonomic profiling

Fecal DNA was extracted using the QIAamp DNA Stool Mini Kit (QIAGEN) following the manufacturer's instructions. Extracted DNA samples were assessed for quality, and those passing quality control were randomly sheared into ~350 bp fragments using a Covaris ultrasonicator. Fragmented DNA underwent end repair, A-tailing, adapter ligation, purification, and PCR amplification to generate sequencing libraries. Libraries that met quality standards were subjected to high-throughput sequencing.

Library preparation and metagenomic shotgun sequencing were performed on the Illumina HiSeq 4000 platform, generating 150 bp paired-end reads with a target depth of >6 Gb per sample (ShenZhen Chi-Biotech Co., Ltd.). Raw reads were processed to remove adapter sequences and low-quality reads. Host-derived contamination was filtered out by aligning reads to the human reference genome (hg38) using Bowtie 2. Taxonomic profiling of the resulting clean reads was conducted using Krona (v2.8.1) with default parameters.

Sparse labeling of hippocampal neurons

Morphological markers of hippocampal neurons used by rAAV-NCSP-YFP-2E5 viruses.[90] The mice were injected into the hippocampus (AP: 1.8 mm from the bregma; LM: 1.1 mm to the sagittal suture; DV: 1.95 mm in depth relative to the skull) using a Hamilton syringe (84851, Hamilton, Bonaduz) at a rate of 20 nL/min (total 100 nL) after the 12th injection. After anesthesia, the mice were placed on the stereotaxic apparatus. Virus was aliquoted and stored at -80°C, and virus titers were greater than 10^{12} virus particles per mL.

Golgi staining

Golgi staining was examined by using the frozen section Neuron Golgi Staining Kit (Genmed Co., Shanghai, China). According to the manufacturer's instructions, mouse brains were immersed in a solution consisting of Solutions A and B (1:1) for 14 days in the dark. Next, the brains were transferred to Solution C for at least 48 h at 4°C in the dark. The brains were then sectioned in a microtome (microtome cryostat 6250, DAKEWE, China) to a thickness of 100 μm. Solutions D and E were used for staining the sections. Finally, the images of dendritic segments were scanned using microscopes (Zeiss Apotome 2, Germany) under brightfield conditions. Dendrite density and length of dendritic spines were quantified with Image J.

UPLC-MS/MS

The intestine was removed after the 12th PTZ injection. The levels of neurotransmitters in intestinal tissues were determined by UPLC-MS/MS. Mice were deeply anesthetised with isoflurane. Intestinal tissue samples were then collected from each mouse and sent to Oebiotech Biotechnology Co., Ltd (Shanghai, China) for analysis. In brief, gut tissue extraction methods were carried out according to the chemical characteristics of multi-targeted metabolites. 500 μL ice-cold acetonitrile-Isopropanol-water (3:3:2, v/v, containing IS) was added into the freeze-dried samples (0.5 mg), then placed into 2 steel balls and grind with a grinder (60 Hz, 2 min). Afterward, the whole samples were extracted by ultrasonic for 10 min in ice-water bath, and samples were placed at -20°C for 30 min. Then centrifuged at 4°C (13,000 rpm) for 10 min and remove 50 μL of supernatant to sample vials. Then the supernatant (50 μL) was dried under a nitrogen stream and re-dissolved in 450 μL of water (containing IS), extracted by ultrasonic for

Please cite this article in press as: Jia et al., Gut-brain cholinergic signaling mediates the antiseizure effects of *Bacteroides fragilis*, Neuron (2025), https://doi.org/10.1016/j.neuron.2025.11.029

5 min in ice-water bath, and then filtered through a 0.22 μm organic phase pinhole filter for subsequent UPLC-MS/MS analysis. Liquid chromatography was performed on an AB ExionLC (AB SCIEX, Framingham, MA). An ACQUITY UPLC HSS PFP (100 mm×2.1 mm, 1.8 μm) was used for analysis. Injection volume was 5 μL. Mass spectrometry was performed on the AB SCIEX Selex ION Triple Quad™ 5500 System, with an electrospray ionization (ESI) source, operating in both positive and negative ion mode. Nitrogen was employed as the collision gas. Intestinal tissue metabolites were analyzed in multiple reaction monitoring (MRM) mode. The MRM pairs, declustering potentials and collision energies were optimized for each analyte. Data acquisitions and further analysis were conducted using Analyst software. SCIEX OS-MQ software was used to quantify all metabolites.

HPLC/MS analysis

The levels of ChAT and GABA in the vagal ganglia, sera and hippocampus were assessed by using HPLC/MS. HPLC/MS analysis was conducted using an Agilent MSD/QTOF 6545 system (Agilent Technologies, Germany) coupled with an HPLC/1290II. The instrument was configured with the following parameters: ESI source nebulizer gas (N2) at a flow rate of 6 L/min, operating at a temperature of 300°C and a pressure of 20 psig. Sheath gas was set to flow at 10 L/min, with a temperature of 320°C, Vcap at 3500 V, skimmer at 65 V, OCT RF at 750 V, fragmentor at 145 V, nozzle at 500 V. Mass scanning was conducted in positive mode within the m/z range of 80–3200, calibrated using online standard reference ions at 121.05 and 922.01. For chemical separation, a mobile phase consisting of water and acetonitrile, both with 0.1% formic acid, was employed to elute the sample from an Agilent Extend 300-C18 column (4.6 × 150 mm, 3.5 μm) at a flow rate of 0.3 ml/min. The gradient elution program spanned 14 min, starting at 3% acetonitrile and increasing to 9% at 10 min, holding at 95% for 3 min, and finally returning to 3%.

Tissue dissection, immunofluorescence, and quantification

Mice were deeply anesthetized with isoflurane and perfused with 4% paraformaldehyde in 0.1 M phosphate-buffered saline (PBS, pH 7.4). The tissues of PTZ-induced mouse model were dissected and fixed in 4% paraformaldehyde for 24 h and transferred to 30% sucrose in PBS. Tissues were sectioned on a microtome (microtome cryostat 6250, DAKEWE) at 35 μm. Tissues slices were stored in cryoprotectant solution (30% sucrose (w/v), 30% ethylene glycol (v/v), 1% PVP-40 (w/v), and 50 mM PBS) at -20°C. After 4 × 10 min washing in PBS containing 0.2% Triton X-100 (PBST), tissues were blocked in 3% normal goat serum (NGS) for 90 min, then incubated in primary antibodies diluted in 3% NGS for 12-24 h at 4°C, then washed in PBST, and incubated in secondary antibodies diluted in 3% NGS for 1–2 days at 4°C. Tissues were then washed thoroughly in PBST and mounted for imaging. Antibodies used were rabbit anti-ZO1 tight junction protein antibody, rabbit anti-Occludin, mouse anti-ChAT, rabbit anti-tyrosine hydroxylase, rabbit synapsin-1, rabbit anti-PGP9.5, mouse anti-pErk1 and secondary Alexa Fluor 488 or 594. Images were acquired using a Zeiss inverted confocal microscope (Zeiss LSM880 Airyscan, Germany) with ×10, ×20 or ×63 objectives and processed using Fiji software. Monochrome images were rendered to emphasize differences in intensity. For each region of interest, a maximum z-projection of a fixed number of image stacks with Occludin signals was created, and the average fluorescence intensity was calculated for each sample. ChAT, Occludin and ZO-1 staining were carefully quantified in each slide by capturing ten randomly chosen fields in a blind manner by two experienced experts. These data were analyzed using software Image J (1.52 v). p-ERK1 immunoreactive cell densities were quantified using unbiased stereology and expressed as the number of positive cells per mm^3. Total cell counts were estimated using DAPI staining, and the proportion of marker-positive cells was calculated relative to total DAPI-positive nuclei within the same volume.[91]

Colon viral injection

The viral constructs (PRV-CAG-EGFP, AAV-ChAT-DIO-EGFP, AAV-ChAT-DIO-hM3Dq-EGFP, AAV-ChAT-DIO-taCasp3-TEVp-EGFP) were loaded into a glass pipette connected to a microsyringe pump (Nanoject III #3-000-207, DRUMNOND). Multiple 0.03 μl injections were made at 0.01 μl/s into each submucosal puncture. Each animal received a total volume of 1μl in the colon. Five days after the viral injection, mice were deeply anesthetized with isoflurane and perfused with 4% paraformaldehyde in 0.1 M phosphate-buffered saline (PBS, pH 7.4). The brain was dissected and fixed in 4% paraformaldehyde for 24 h and transferred to 30% sucrose in PBS. And sectioned on a microtome (microtome cryostat 6250, DAKEWE) at 35 μm. Brain slices were stored in cryoprotectant solution (30% sucrose (w/v), 30% ethylene glycol (v/v), 1% PVP-40 (w/v), and 50 mM PBS) at -20°C. After 4 × 10 min washing in PBS, brain was then washed thoroughly in PBST and mounted for imaging.

NG viral injection

The vagus nerve was separated from the carotid artery with a surgical hook (RWD Life Science, China) until the jugular-NG became accessible. Viral aliquots (AAV-Retro-CAG-EGFP, RV-EnvA-ΔG-mCherry-Cre, AAV-hSyn-T2A-TVA, AAV-hSyn-RVG) were loaded into a glass pipette connected to a microsyringe pump (Nanoject III #3-000-207, DRUMNOND). For each NG, a total 0.5 μl volume was delivered into two sites, rostral and caudal to the laryngeal nerve branch, at 0.2 μl/min using a glass pipette mounted on a microsyringe pump (Nanoject III #3-000-207, DRUMNOND). After 4 weeks, mice were deeply anesthetized with isoflurane and perfused with 4% paraformaldehyde in 0.1 M phosphate-buffered saline (PBS, pH 7.4). The gut and NG were dissected and fixed in 4% paraformaldehyde for 24 h and transferred to 30% sucrose in PBS. And sectioned on a microtome (microtome cryostat 6250, DAKEWE) at 35 μm. Gut and NG slices were stored in cryoprotectant solution (30% sucrose (w/v), 30% ethylene glycol (v/v), 1% PVP-40 (w/v), and 50 mM PBS) at -20°C. After 4 × 10 min washing in PBS, NG were then washed thoroughly in PBST and mounted for imaging. Gut

slices were blocked in 3% normal goat serum (NGS) for 90 min, then incubated in mouse anti-ChAT diluted in 3% NGS for 12-24 h at 4°C, then washed in PBST, and incubated in secondary antibodies diluted in 3% NGS for 1–2 days at 4°C. Gut slices were then washed thoroughly in PBST and mounted for imaging.

Unilateral cervical vagotomy

Mice were anesthetised with isoflurane. A midline abdominal incision was made through the skin and muscle. An incision was made in the neck to expose the esophagus, and the left vagal ganglia branches were gently pulled apart from the esophagus to expose them. The vagal trunks were resected. Control mice received sham surgery, which included all surgical procedures except vagotomy.

Vagus nerve stimulation

Mice were deeply anesthetised with isoflurane and a bipolar cuff electrode (300 μm cuffs, 2 channels, Samtec16 connector, Kedou Brain-computer Technology Co., Ltd, Suzhou, China) was implanted on the vagal nerve. The vagal nerve was accessed through a ventral cervical incision and the nerve was bluntly dissected from the carotid sheath. The cuff was tunneled subcutaneously from an incision at the base of the dorsal skull to the ventral cervical incision. The vagal nerve was placed in the cuff. The ventral cervical incision was sutured with 6-0 absorbable sutures. The dorsal skull was cleaned with saline and ethanol, and electrical connectors were fixed to the skull with dental cement (19-7220, HUAYON Technology Co., Ltd, Shenzhen, China). Stimulation efficacy was measured using peripheral biomarkers such as changes in respiratory rate and heart rate reduction on the day of surgery.[92] Mice were monitored for 7 days to ensure proper recovery from surgery before subsequent experiments. For all VNS experimental groups, VNS was set at 10 Hz with a pulse width of 0.5 ms, which was cycled continuously for 5 min. Current amplitudes were 0.1 mA. Stimulation parameters were controlled and delivered using a RIGOL DHO800 system (RIGOL Technologies, Beijing, China) connected to a stimulation isolation unit (A-M Systems, Model 2200 analogue stimulus isolator, USA) to control the current. After 10 PTZ injections, VNS was performed 30 min before the final injection.

Vagus nerve recording

For vagal nerve activity recording, the bipolar cuff electrode (300 μm cuffs, 2 channels, Samtec16 connector, Kedou Brain-computer Technology Co., Ltd, Suzhou, China) was used. The implantation procedure is the same as for vagal nerve stimulation. The bipolar cuff electrode has the function of recording the electrogram using the Apollo II high-throughput neural recording system.

Vagus nerve recording during a seizure

After a 7-day recovery period, we officially commenced this experiment. Prior to the administration of PTZ (pentylenetetrazol), we first recorded the basal vagus nerve firing rate of the mice while they were in a conscious state. Immediately after, we administered a 30 mg/kg solution of PTZ to the mice and continuously monitored changes in their vagus nerve firing rate for the next half hour.

Vagus nerve recordings under different treatments

Vagus nerve recordings under different treatments were performed in wild-type mice. The mice were anesthetized with 2.5% isoflurane delivered in 100% oxygen and positioned supine. During surgical procedures, the isoflurane concentration was maintained at 2.0%. Following successful isolation of the target nerve, the anesthesia level was reduced to approximately 1.75% isoflurane for electrophysiological recordings.[61] The implantation the cuff recording electrode in vagus nerve procedure is the same as for vagal nerve stimulation. Next, a 20-gauge gavage needle with three connected tubes for saline perfusion, ACh and BF839 delivery was surgically inserted through the stomach wall into the proximal colon distal to the cecum. A perfusion exit incision was made at the proximal to the rectum for colon. Saline was constantly perfused through the isolated intestinal region at ∼400 μl/min as a within-subject baseline and volume pressure control. Stimulation conditions were applied after recording 2 min of baseline activity. During ACh/ BF839 stimulation conditions, saline perfusion was continuous, and 200 μl of stimulant was delivered 1 min with a glass pipette connected to a microsyringe pump (Nanoject III #3-000-207, DRUMNOND). The 1-min infusions of each stimulation were separated by at least 6 min or the return to baseline firing rate, whichever came first. Throughout experiments, ACh response was used as a positive control. For all stimulation conditions, data were excluded if a stable ACh response was not seen throughout the recording session. Each mouse received different stimulations in addition to the ACh positive control. All stimulations were dissolved in PBS. The following final concentrations for each infused stimulation were used: 5mM ACh, 1 x 10^9 CFU BF839, 1 mM mecamylamine.

Data acquisition and analysis

The spike detection method was adapted from vagal nerve activity signals and analysed using Neuroexplorer software.[93] The firing rate was calculated using a Gaussian kernel smoothing algorithm in 200-ms bins. Each trial the firing rate was normalized to the average firing rate of the saline over 10 min to serve as its own control.

Intrahippocampal kainic acid injection

Mice were anesthetized with isoflurane (5% for induction, 2% for maintenance) and placed in a stereotaxic frame. A midline scalp incision was made to expose the skull, and cranial sutures (bregma and lambda) were identified. A burr hole was drilled above the right hippocampus (coordinates: −2.0 mm anteroposterior (AP), +1.5 mm mediolateral (ML) relative to bregma). Kainic acid (KA; 200 ng in 50 nl saline, Bio-Techne) was injected into the dorsal hippocampus (−1.8 mm dorsoventral (DV) from the dura) using a Hamilton Neuros syringe (Nanoject III #3-000-207, DRUMMOND) mounted on an automated injection pump at a rate of 100 nl/min.

Please cite this article in press as: Jia et al., Gut-brain cholinergic signaling mediates the antiseizure effects of *Bacteroides fragilis*, Neuron (2025), https://doi.org/10.1016/j.neuron.2025.11.029

Following infusion, the needle was left in place for 5 min before being slowly withdrawn, after which the incision was closed to complete the surgery. Throughout the procedure, body temperature was maintained at 37°C using a thermoregulated heating pad. As a result of KA injection, mice developed status epilepticus and exhibited behavioral seizures post-surgery.

Immunohistochemical analysis

At 3 h after the EEG experiment, mice were transcardially perfused with saline, and brains were dissected and post-fixed in 4% paraformaldehyde for 24 h at 4°C. Brain tissue was embedded in paraffin and sectioned into 5-μm coronal slices. For histological analysis, immunohistochemistry was performed using antibodies including c-Fos (1:200). For c-Fos immunohistochemistry, we followed an established protocol based on previous research.[94,95] Sections were preincubated with 3% H_2O_2 in PBS for 15 min at 25°C to quench endogenous peroxidase activity, followed by three washes with PBS (10 min each). Blocking was done with 2.5% NGS in PBS containing 0.1% Tween 20 for 1 h. Sections were then incubated with mouse anti-c-Fos antibody (1:300; ab208942, Abcam) diluted in PBS with 2.5% NGS and 0.1% Tween 20 overnight at 4°C. After washing, sections were incubated with biotinylated anti-mouse IgG (1:300; Vector Laboratories) for 2 h at 25°C, followed by ABC kit (Vector Laboratories) treatment according to manufacturer instructions. Signal was developed using diaminobenzidine (DAB) substrate (Vector Laboratories), and sections were washed, dried, and mounted. Stained sections were scanned with a Pannoramic MIDI whole-slide scanner (3DHISTECH, Budapest, Hungary), and images of the CA1, CA3, and DG regions were acquired using SlideViewer software.

Chemogenetic manipulation of the colonic ChAT$^+$–vagus nerve pathway

We used a Cre-dependent taCasp3-based ablation vector (AAV-DIO-taCasp3-TEVp-EGFP) to selectively ablate ChAT$^+$ cells. Viral vectors were used to express either the control fluorophore EGFP or the engineered caspase-3 variant (taCasp3). taCasp3 contains a TEV protease (TEVp) recognition motif inserted at its intrinsic cleavage site (between residues D175 and S176). Co-expression of TEVp activates taCasp3 through site-specific proteolysis, thereby inducing apoptosis in targeted neurons.

For chemogenetic activation, we used an AAV-ChAT-DIO-hM3Dq-EGFP viral vector, which enhances neuronal activity upon administration of a designer drug. EGFP, taCasp3-TEVp, or hM3Dq were selectively expressed in colonic ChAT$^+$ cells using a Cre-dependent dual-virus strategy. Specifically, the colon was infused with AAVs carrying double-floxed inverted open reading frames (AAV-ChAT-DIO-EGFP, AAV-ChAT-DIO-taCasp3-TEVp-EGFP, or AAV-ChAT-DIO-hM3Dq-EGFP), while the vagus nerve was infused with a retrograde rabies virus (RV) vector encoding Cre recombinase (RV-EnvA-ΔG-mCherry-Cre) together with helper viruses (AAV-hSyn-TVA and AAV-hSyn-N2cG). Viral volumes of ∼200–500 nL were delivered per site at a rate of 5 nL/s. Following RV injection, viral expression was allowed for 3–5 days before behavioral testing. hM3Dq was activated by systemic administration of the designer drug Deschloroclozapine (DCZ), prepared in 5% DMSO and 0.9% saline. Intraperitoneal injections (1 mg/kg) were performed 5–10 min before PTZ-induced seizures or vagus nerve recordings to induce neuronal activation.

The co-cultivation of *B. fragilis* and *L. reuteri*

BF839 and *L. reuteri* were co-cultured on a tissue culture plate insert (Guangzhou Jet Bio-Filtration Co., Ltd. TCS-016-012, 0.4 μm) with two compartments separated by a polycarbonate membrane with a pore size of 0.4 μm, enabling metabolic exchange between BF839 and *L. reuteri* through the polycarbonate membrane. BF839 was located in the inner chamber while *L. reuteri* was placed in the outer chamber, as illustrated in Figure 6T. The initial inoculum size for BF839 was 1 OD, whereas for *L. reuteri*, it ranged from 0 to 0.05 OD. Subsequently, every 24 h, corresponding bacterial suspensions were added into the new chamber until 96 h, and then the OD values of bacterial suspensions at each time point were measured using Enzyme-linked immunosorbent assay (Tecan infinite M200 Pro, Switzerland) reader of 600 nm.

In vivo co-cultivation of BF839 and *L.reuteri* was conducted by administering mice with BF839 (1×10^9 CFU), *L. reuteri* (1×10^9 CFU), and a mixed solution containing BF839 (5×10^8 CFU) and *L. reuteri* (5×10^8 CFU) daily for 5 consecutive days. Subsequently, fresh mice feces from each group of mice were weighed, and 1g of feces was placed into a centrifuge tube. Sterile physiological saline (200 μL) was added and mixed through grinding. After homogenizing the feces for 2 min at 8000 r/min, they were centrifuged for 30 s at 1000 rpm to separate the supernatants. These supernatants underwent seven sequential 1/10 dilutions and were plated onto MRS agar. The plates were incubated at 37°C under anaerobic conditions. For identification, three colonies were randomly selected from each plate and subjected to 16S rRNA gene PCR using the primers 338F (5'-ACTCCTACGGGAGGCAGC-3') and 806R (5'- GGACTACHVGGGTWTCT AAT-3'). The resulting 16S rRNA gene sequences were analyzed using BLAST to determine their identity. This identification process was performed to confirm the presence of *L. reuteri*, in the feces following the *in vivo* co-cultivation experiment described previously.

The co-culture of *L. reuteri* with BF839 and *E. coli* separately in nutrient plate supplemented with 0.5% yeast extract. Dilute *L. reuteri*, BF839, and *E. coli* with an initial concentration of 1 ± 0.2 OD by a factor of 1,000,000. Then, take 100 μL of both BF839 and *E. coli* and mix them separately with *L. reuteri* for plating using nutrient agar medium at 37°C under anaerobic conditions for 96 h. Three randomly selected colonies in the plate were identified by 16S rRNA gene PCR with using primers 338F (5'-ACTCCTACGGGAGGCAGC-3') and 806R (5'- GGACTACHVGGGTWTCTAAT-3'). 16S rRNA gene sequence data was characterized by BLAST analysis.

Metabolic predictions

The microbial community metabolic modeling (MICOM) was used to predict the metabolic output of individual gut microbial communities.[63] All metagenome-scale metabolic models were built with AGORA genus model database (agora201_gtdb207_genus.qza)

and the standard diet gut medium (COBRApy package).[96] Community growth rates were optimized using MICOM's cooperative trade-off strategy, which balances individual taxon growth and overall community growth. The optimal trade-off value was identified using the trade-off function and applied in subsequent growth simulations with the grow function. The resulting models provided individual and community-level growth rates as well as predicted fluxes of metabolite production and consumption (reported in mmol/[gDW·h]).

Clinical observational study

Interventions

The treatment plan for BF839 is as follows: (1) Treatment group: The children received BF839 as directed, with dosages determined according to their age. Children under 3 years of age were administered half of a sachet in the morning and evening. Children aged between 3–6 years were administered one sachet (4×10^9 CFU) in the morning and half of a sachet in the evening. For children aged over 6 years, they were administered one sachet in the morning and evening. BF839 was dissolved in warm water at 45°C. The treatment duration was 3 months. (2) Placebo group: The children were instructed to take a placebo (100% Maltodextrin, 10g/per time) as required, with the dose determined by age. Those aged under 3 years were administered half of a sachet in the morning and evening. Those aged between 3–6 years old were administered one sachet in the morning and half of a sachet in the evening. For those aged over 6 years, they were administered one sachet in the morning and evening. The placebo was dissolved in warm water at 45°C. The treatment duration was 3 months. The placebo group received compensation with a trial of BF839 after the end of the study. The children had to maintain the original antiseizure medication regimens for 1 month before and after enrollment. Moreover, the children were not allowed to take other types of probiotics supplements during the trial. In line with the principle of protecting the safety of the participants, if a child developed status epilepticus, serious adverse reactions, or a significant increase in seizure frequency during the study, the trial could be discontinued with the investigator's consent, and the appropriate treatment would be provided.

Outcomes

The primary outcome measure of the BF839 clinical trial is efficacy rate of seizure frequency reduction. Changes in seizure frequency regarding the major seizure types were assessed monthly (28 days) from baseline to 3 months after probiotics treatment. Efficacy was defined as the proportion of participants who achieved either a $\geq$50% reduction in seizure frequency or complete seizure cessation. Secondary outcomes included changes in gut microbiota composition assessed by 16S rRNA sequencing.

Sample size estimation

Due to the impact of the global COVID-19 pandemic, we re-evaluated the sample size and adjusted the anticipated loss-to-follow-up rate. According to the results of existing clinical studies, we assumed an efficacy rate of 42.9%[97] for the experimental group and 5%[98] for the control group; 19 participants per group were needed at 5% significance with 85% power. Taking into account a 35% loss-to-follow-up rate, we estimated the sample size to 60 participants.

QUANTIFICATION AND STATISTICAL ANALYSIS

Statistical analyses

For animal experiments, quantitative analyses were performed using Prism 8.0 or Origin 2024, as indicated in each figure legend. Data distributions were evaluated for normality and are presented as mean ± SEM. For each figure, *n* refers to the number of independent biological replicates. Normality was assessed using the D'Agostino-Pearson test. For normally distributed data, two-tailed Student's *t* tests were used for comparisons between two groups, and one-way ANOVA followed by Tukey's multiple-comparisons test was used for comparisons across multiple groups. For non-normally distributed data, two-tailed Mann-Whitney U tests or Welch's *t* tests were used for two-group comparisons, and Kruskal-Wallis tests followed by Dunn's multiple-comparisons test were applied for comparisons among three or more groups. Categorical variables were summarized as frequencies and percentages, and group differences were assessed using chi-squared or Fisher's exact tests.

For the clinical study, data were analyzed using SPSS 24.0 without imputation for missing values, as no reliable imputation method exists for 16S rRNA sequencing data; patients lost to follow-up were excluded from analysis. Normally distributed continuous variables are presented as mean ± standard deviation and analyzed using two-tailed Student's *t* tests. Non-normally distributed variables are presented as median (interquartile range) and analyzed using two-tailed Mann-Whitney U tests. Categorical variables are reported as counts (percentages) and analyzed using Fisher's exact test, which was applied to the primary efficacy endpoint (seizure frequency reduction rate). Gut microbiota data in figures are displayed as mean ± SEM. Normality was assessed using the D'Agostino-Pearson test. Statistical significance was defined as $p < 0.05$.

Image preparation

EEG data were analyzed and visualized using MATLAB 2019, and three-dimensional image reconstruction was performed with Imaris Viewer 10. All images and figure layouts were prepared using Adobe Illustrator CC 2019.